participate in the higher order function of the nervous system during adulthood in a manner that can be detected by impaired motor coordination in mice deficient for NB-3 or Punc.

Excitatory Transmission at the CF and PF Synapses Is Normal in the NB-3 Mutant Mice

Electrophysiological analyses can provide clues about whether such defects in the knockout mice are due to the impairment of cerebellar synaptic transmission. NB-3 knockout mice had normal monosynaptic CF innervation, conductance of CF synapses to Purkinje cells, and paired-pulse plasticity of CF- and PF-mediated EPSCs in all lobules. Electron microscopic observations that revealed well-developed Purkinje cell dendrites and parallel fibers also showed morphologically refined synapse organization. These results might indicate that NB-3 is not essentially involved in the excitatory synaptic transmission to Purkinje cells. Alternatively, the output from Purkinje cells to the vestibular nucleus may be impaired. The descending pathway from the cerebellar cortex is only an inhibitory output via Purkinje cell axons that innervate the vestibulocerebellum (Ito et al., 1964). An important function of the vestibulocerebellum is higher regulation of the vestibulospinal reflex. It has been reported that contactin subgroup molecules are mainly localized on axons (Yoshihara et al., 1994, 1995). If NB-3 is localized on Purkinje cell axons and/or cells in the descending pathway, signal transmission to the vestibular nucleus might be impaired without any influence on CF- or PF-EPSCs. Another reason for the defect of motor coordination may be impairment of mossy fiber innervation. Mossy fibers are originated from several regions such as the vestibular nucleus, pontine reticular nucleus, and spinal cord. These areas express a significant amount of NB-3 transcripts (Lee et al., 2000), so that lack of NB-3 might affect the excitatory synaptic transmission to either granule cells or Golgi cells. Although we have reported the localization of NB-3 transcripts by *in situ* hybridization in the rat brain (Lee et al., 2000), and here identified the cells producing NB-3 proteins in the cerebellum through the expression of Lac Z, the NB-3 protein localization at the cellular level in the cerebellum has not yet been determined. It will be essential to know the NB-3 protein localization at the cellular level to the electrophysiology of the knockouts.

Recent studies have shown that contactin plays essential roles in the formation and maintenance of paranodal regions in coordination with caspr in the PNS (Bhat et al., 2001; Boyle et al., 2001). The synaptic transmission at myelinated neurons is impaired in contactin and caspr knockout mice. Similarly, it is highly possible that NB-3 is localized at the regions proximal to the node, including the paranode, of the CNS, because contactin and NB-3 are in the same subgroup of proteins. In this respect, detailed analyses of the NB-3 knockout mice, which exhibit defects in motor coordination, will provide important tools for understanding the molecular mechanism underlying the neural function performed by NB-3.

We are greatly indebted to Drs. Nomoto, Miyasaka and Ohta in our Institute for the rotorod apparatus. We also thank Ms. Sugiura for an excellent technical support for electronmicroscopy, and Mr. Fujita for an outstanding photography.

REFERENCES

Aiba A, Kano M, Chen C, Stanton ME, Fox GD, Herrup K, Zwingman TA, Tonegawa S. 1994. Deficient cerebellar long-term depression and impaired motor learning in mGluR1 mutant mice. Cell 79:377–388.

Berglund EO, Murai KK, Fredette B, Sekerkova G, Marturano B, Weber L, Mugnaini E, Ranscht B. 1999. Ataxia and abnormal cerebellar microorganization in mice with ablated contactin gene expression. Neuron 24:739–750.

Bhat MA, Rios JC, Lu Y, GarciaFresco GP, Ching W, St Martin M, Li JJ, Einheber S, Chesler M, Rosenbluth J, et al. 2001. Axon-glia interactions and the domain organization of myelinated axons requires Neurexin IV/Caspr/Paranodin. Neuron 30:369–383.

Boyle ME, Berglund EO, Murai KK, Weber L, Peles E, Ranscht B. 2001. Contactin orchestrates assembly of the septate-like junctions at the paranode in myelinated peripheral nerve. Neuron 30:385–397.

Callahan CA, Thomas JB. 1994. Tau-β-galactosidase, an axon-targeted fusion protein. Proc Natl Acad Sci USA 91:5972–5976.

Corriveau RA, Huh GS, Shatz CJ. 1998. Regulation of class I MHC gene expression in the developing and mature CNS by neural activity. Neuron 21:505–520.

Cremer H, Lange R, Christoph A, Plomann M, Vopper G, Roes J, Broen R, Baldwin S, Kraemer P, Scheff S, et al. 1994. Inactivation of the N-CAM gene in mice results in size reduction of the olfactory bulb and deficits in spatial learning. Nature 367:455–459.

Crepel F. 1992. Regression of functional synapses in the immature mammalian cerebellum. Trends Neurosci 5:266–269.

Dean RLI, Scozzafava J, Goas JA, Regan B, Beer B, Bartus RT. 1981. Age-related differences in behavior across the life span of the C57BL/6J mouse. Exp Aging Res 7:427–451.

Doherty P, Fazeli MS, Walsh FS. 1995. The neural cell adhesion molecule and synaptic plasticity. J Neurobiol 26:437–446.

Edwards FA, Konnerth A, Sakmann B, Takahashi T. 1989. A thin slice preparation for patch clump recordings from neurones of the mammalian central nervous system. Pflugers Arch 414:600–612.

Ferguson GD, Anagnostaras SG, Silva AJ, Herschman HR. 2000. Deficits in memory and motor performance in synaptotagmin IV mutant mice. Proc Natl Acad Sci USA 97:5598–5603.

Horai R, Saijo S, Tanioka H, Nakae S, Sudo K, Okahara A, Ikuse T, Asano M, Iwakura Y. 2000. Development of chronic inflammatory arthropathy resembling rheumatoid arthritis in interleukin 1 receptor antagonist-deficient mice. J Exp Med 191:313–320.

Ito M, Yoshida M, Obata K. 1964. Monosynaptic inhibition of the intracerebellar nuclei induced rom the cerebellar cortex. Experientia 20:575–576.

Itoh K, Stevens B, Schachner M, Fields RD. 1995. Regulated expression of the neural cell adhesion molecule L1 by specific patterns of neural impulses. Science 270: 1369–1372.

Kano M, Rexhausen U, Dreessen J, Konnerth A. 1992. Synaptic excitation produces a long-lasting rebound potentiation of inhibitory synaptic signals in cerebellar Purkinje cells. Nature 256:601–604.

Kiss JZ, Wang C, Olive S, Rougon G, Lang JC, Baetens D, Harry D, Pralong WF. 1994. Activity-dependent mobilization of the adhesion molecule polysialic NCAM to the cell surface of neurons and endocrine cells. EMBO J 13:5284–5292.

Lee S, Takeda Y, Kawano H, Hosoya H, Nomoto M, Fujimoto D, Takahashi N, Watanabe K. 2000. Expression and regulation of a gene encoding neural recognition molecule NB-3 of the contactin/F3 subgroup in mouse brain. Gene 245:253–266.

Llano I, Marth A, Armstrong CM, Konnerth A. 1991. Synaptic- and agonist-induced excitatory currents of Purkinje cells in rat cerebellar slices. J Physiol (Lond) 434:183–213.

Mayeux-Portas V, File SE, Stewart CL, Morris RJ. 2000. Mice lacking the cell adhesion molecule Thy-1 fail to use socially transmitted cues to direct their choice of food. Curr Biol 10:68–75.

Mayford M, Barzilai A, Keller F, Schacher S, Kandel ER. 1992. Modulation of an NCAM-related adhesion molecule with long term synaptic plasticity in *Aplysia*. Science 256:638–644.

Murase S, Schuman EM. 1999. The role of cell adhesion molecules in synaptic plasticity and memory. Curr Opin Cell Biol 11:549–553.

Ogawa J, Kaneko H, Masuda T, Nagata S, Hosoya H, Watanabe K. 1996. Novel neural adhesion molecules in the Contactin/F3 subgroup of the immunoglobulin superfamily: isolation and characterization of cDNAs from rat brain. Neurosci Lett 218:173–176.

Ogawa J, Lee S, Itoh K, Nagata S, Machida T, Takeda Y, Watanabe K. 2001. Neural recognition molecule NB-2 of the contactin/F3 subgroup in rat: specificity in neurite outgrowth-promoting activity and restricted expression in the brain regions. J Neurosci Res 65(2):100–110.

Raymond JL, Lisberger SG, Mauk MD. 1996. The cerebellum: a neuronal learning machine? Science 272:1126–1131.

Storm DR, Hansel C, Hacker B, Parent A, Linden DJ. 1998. Impaired cerebellar long-term potentiation in type 1 adenylyl cyclase mutant mice. Neuron 20:1199–1210.

Theodosis DT, Bonhomme R, Vitiello S, Rougon G, Poulain DA. 1999. Cell surface expression of polysialic acid on NCAM is a prerequisite for activity-dependent morphological neuronal and glial plasticity. J Neurosci 19: 10228–10236.

Yang W, Li C, Mansour SL. 2001. Impaired motor coordination in mice that lack punc. Mol Cell Biol 21:6031–6043.

Yoshihara Y, Kawasaki M, Tamada A, Nagata S, Kagamiyama H, Mori K. 1995. Overlapping and differential expression of BIG-2, BIG-1, TAG-1, and F3: four members of an axon-associated cell adhesion molecule subgroup of the immunoglobulin superfamily. J Neurobiol 28:51–69.

Yoshihara Y, Kawasaki M, Tani A, Tamada A, Nagata S, Kagamiyama H, Mori K. 1994. BIG-1: a new TAG-1/F3-related member of the immunoglobulin superfamily with neurite outgrowth-promoting activity. Neuron 13:415–426.

Article

Association of TAG-1 with Caspr2 is essential for the molecular organization of juxtaparanodal regions of myelinated fibers

Maria Traka,[1] Laurence Goutebroze,[2] Natalia Denisenko,[2] Maria Bessa,[1] Artemisia Nifli,[1] Sophia Havaki,[3] Yoichiro Iwakura,[4] Fumihiko Fukamauchi,[5] Kazutada Watanabe,[6] Betty Soliven,[7] Jean-Antoine Girault,[2] and Domna Karagogeos[1]

[1]Department of Basic Science, University of Crete Medical School and Institute of Molecular Biology and Biotechnology (IMBB), 71110 Heraklion, Greece
[2]Institut National de la Santé et de la Recherche Medicale U 536, Université Pierre et Marie Curie (UPMC), Institut du Fer à Moulin, 75005 Paris, France
[3]Neurobiology Research Institute, Cozzika Foundation, 11528 Athens, Greece
[4]Center for Experimental Medicine, Institute of Medical Science, University of Tokyo, 108-8639 Tokyo, Japan
[5]Department of Molecular Medical Science, Medical Research Institute, Tokyo Medical and Dental University, Tokyo and Tsukuba College of Technology, 305-005 Ibaraki, Japan
[6]Department of BioEngineering, Nagaoka University of Technology, 940-21 Nagaoka, Japan
[7]Department of Neurology, University of Chicago, Chicago, IL 60637

Myelination results in a highly segregated distribution of axonal membrane proteins at nodes of Ranvier. Here, we show the role in this process of TAG-1, a glycosyl-phosphatidyl-inositol–anchored cell adhesion molecule. In the absence of TAG-1, axonal Caspr2 did not accumulate at juxtaparanodes, and the normal enrichment of *shaker*-type K^+ channels in these regions was severely disrupted, in the central and peripheral nervous systems. In contrast, the localization of protein 4.1B, an axoplasmic partner of Caspr2, was only moderately altered. TAG-1, which is expressed in both neurons and glia, was able to associate in cis with Caspr2 and in trans with itself. Thus, a tripartite intercellular protein complex, comprised of these two proteins, appears critical for axo–glial contacts at juxtaparanodes. This complex is analogous to that described previously at paranodes, suggesting that similar molecules are crucial for different types of axo–glial interactions.

Introduction

Myelinated axons in the central and peripheral nervous systems (PNSs) are organized into distinct domains as a consequence of their interactions with glial cells (Vabnick et al., 1997; Kaplan et al., 1997, 2001; Dupree et al., 1999; Mathis et al., 2001; Arroyo et al., 2002). Paranodal junctions separate the nodes of Ranvier from internodal regions. At their level, the extremities of compact myelin wraps expand in a series of cytoplasm-filled loops, which adhere to the neuronal plasma membrane, or axolemma, forming septate-like axo–glial junctions. Several adhesion proteins have been localized at these junctions (for reviews see Peles and Salzer, 2000; Girault and Peles, 2002; Scherer and Arroyo, 2002). In the paranodal axolemma, paranodin/Caspr, a member of the neurexin IV-caspr-paranodin (NCP) group of the neurexin superfamily, is associated with contactin/F3, a cell adhesion molecule of

M. Traka and L. Goutebroze contributed equally to this work.

Address correspondence to Domna Karagogeos, Institute of Molecular Biology and Biotechnology, P.O. Box 1527, Vassilika Vouton, Heraklion 711 10, Crete, Greece. Tel.: 30-28-81-39-45-42. Fax: 30-28-81-39-45-30. email: karagoge@nefeli.imbb.forth.gr

M. Traka's present address is Department of Neurology, University of Chicago, 5841 South Maryland Ave., MC2030, Chicago, IL 60637-1470.

Key words: TAG-1/axonin-1/contactin-2; paranodin/Caspr/NCP-1; potassium channels; protein 4.1B; nodes of Ranvier

Abbreviations used in this paper: CMAP, compound muscle action potential; CNS, central nervous system; GPI, glycosylphosphatidylinositol; IB, immunoblot; IF, immunofluorescence; IgSF, Ig superfamily; IP, immunoprecipitation; IR, immunoreactivity; MAG, myelin-associated glycoprotein; NCP, neurexin IV-caspr-paranodin; P8, postnatal day 8; PNS, peripheral nervous system.

The Journal of Cell Biology, Volume 162, Number 6, September 15, 2003 1161–1172
http://www.jcb.org/cgi/doi/10.1083/jcb.200305078

the immunoglobulin superfamily (IgSF; Einheber et al., 1997; Menegoz et al., 1997; Rios et al., 2000). Contactin/F3, a glycosylphosphatidylinositol (GPI)-linked protein, is necessary for recruiting paranodin/Caspr to the plasma membrane and for its targeting to the paranodes (Faivre-Sarrailh et al. 2000; Rios et al., 2000; Boyle et al., 2001). The complex formed by these two proteins interacts with the 155-kD isoform of neurofascin (NF155), another IgSF protein expressed by glial cells and concentrated in paranodal loops (Tait et al., 2000; Charles et al., 2002). In the absence of either paranodin/Caspr or contactin/F3 paranodal junctions are severely altered and loose their septate-like appearance (Bhat et al., 2001; Boyle et al., 2001). Thus, these three proteins are thought to form an intercellular complex linking the glial plasma membrane to the axolemma and are necessary for the formation of septa (for review see Girault and Peles, 2002). These transmembrane intercellular complexes interact with axoplasmic proteins through the cytoplasmic region of paranodin/Caspr which encompasses a glycophorin C-neurexin IV-paranodin–binding motif for the protein 4.1 family (Menegoz et al., 1997; Girault et al., 1998). Protein 4.1B has been recently identified as a major cytoplasmic partner of paranodin/Caspr at paranodes and may provide an anchor to the actin/spectrin based axonal cytoskeleton (Ohara et al., 2000; Gollan et al., 2002; Denisenko-Nehrbass et al., 2003b).

The *shaker*-type delayed-rectifier potassium channels subunits, Kv1.1 and Kv1.2, are clustered in juxtaparanodal regions (Wang et al., 1993). Although their function remains largely unknown, the localization of K^+ channels at juxtaparanodes may stabilize conduction and maintain the internodal resting potential (Zhou et al., 1998; Vabnick et al., 1999). Caspr2, a member of the NCP family, closely related to paranodin/Caspr (45% amino acid identity), is also enriched in the juxtaparanodal axolemma (Poliak et al., 1999). Caspr2 can be coimmunoprecipitated with K^+ channels, and their interaction may involve a protein with PDZ domains (Poliak et al., 1999), yet to be identified (Rasband et al., 2002). Caspr2 cytoplasmic domain encompasses a glycophorin C-neurexin IV-paranodin motif and associates in vitro and in vivo with protein 4.1B that is also present at juxtaparanodes (Denisenko-Nehrbass et al., 2003b). However, it is not known whether Caspr2 is associated with other axonal membrane protein(s) and whether it interacts with glial proteins.

Recently, TAG-1, an IgSF protein closely related to contactin/F3 (50% amino acid identity) was found to be enriched in juxtaparanodal regions of central nervous system (CNS) and PNS myelinated fibers (Traka et al., 2002). TAG-1, which exists in neurons as a GPI-anchored protein and as a secreted form, was originally described as a protein transiently expressed in axons during development of rodents (Dodd et al., 1988; Furley et al., 1990; Karagogeos et al., 1991). The protein is also expressed by oligodendrocytes and Schwann cells, the myelinating glial cells of the CNS and PNS, respectively (Traka et al., 2002). TAG-1 immunoreactivity (IR) is colocalized with Kv1.1 channels and Caspr2 (Traka et al., 2002), but it is not known whether and how these proteins interact.

Here, we have investigated the function of TAG-1 in axo–glial contacts by analyzing the phenotype of TAG-1–deficient mice and observed that the distribution of juxtaparanodal proteins, Caspr2 and K^+ channels, was severely altered in the CNS and PNS of the mutant mice. We have also examined the interactions between TAG-1 and Caspr2 in brain and in transfected cells, and found that TAG-1 and Caspr2 are able to associate. Thus, this paper reveals that proteins of the NCP family and GPI-anchored IgSF cell adhesion molecules form conserved complexes important for the organization of markedly distinct axonal domains in nodal regions of myelinated fibers.

Results

The basic ultrastructural organization of myelinated fibers and nerve function are preserved in TAG-1 mutant mice

TAG-1–deficient mice survive and reproduce normally (Fukamauchi et al., 2001). Although mutant mice display a greater sensitivity to pro-convulsant stimuli and a marked elevation of adenosine A1 receptors in the hippocampus, morphological analysis of the cerebellum, spinal cord, and hippocampus of these mice did not reveal gross abnormalities (Fukamauchi et al., 2001). Because TAG-1 is also expressed in oligodendrocytes, we examined whether the absence of TAG-1 altered the ultrastructural organization of myelinated axons by electron microscopy. In ultrathin transverse spinal cord sections, myelin sheath thickness and compaction were similar in myelinated fibers of the ventral spinal cord region of wild-type (Fig. 1 A) and TAG-1 mutant mice (Fig. 1 B). The nodal, paranodal, and juxtaparanodal regions appeared properly organized in spinal cord sections of both wild-type (Fig. 1 C) and mutant animals (Fig. 1 D). Finally, the transverse bands, the hallmarks of normal axo–glial junctions, were normally present in both genotypes (Fig. 1, E and F, arrowheads). These results show that TAG-1 expression is not required for myelin sheath formation and structural organization of distinct axonal domains.

We also examined whether the absence of TAG-1 would result in abnormal nerve function by performing basic electrophysiological studies on sciatic nerves of 2-mo-old wild-type and mutant mice. Compound muscle action potentials (CMAPs) recorded after distal and proximal stimulation of sciatic nerves, and F waves, which represent late responses from antidromically activated motor neurons, were similar in both genotypes (Fig. 1, G and H). There was no difference in CMAP amplitudes, distal latencies or conduction velocities between wild-type, heterozygous, and homozygous TAG-1 mutant nerves (Table I). In addition, there was no evidence of partial conduction block or temporal dispersion that would indicate the presence of a demyelinating neuropathy. Altogether these findings indicated the absence of major morphological and functional deficit in the myelinated fibers of TAG-1 knockout mice.

Distribution of juxtaparanodal proteins is dramatically altered in the CNS of TAG-1–deficient mice

We examined whether the absence of TAG-1 altered axo–glial interactions at the molecular level by studying the localization of markers of nodal regions by immunofluorescence

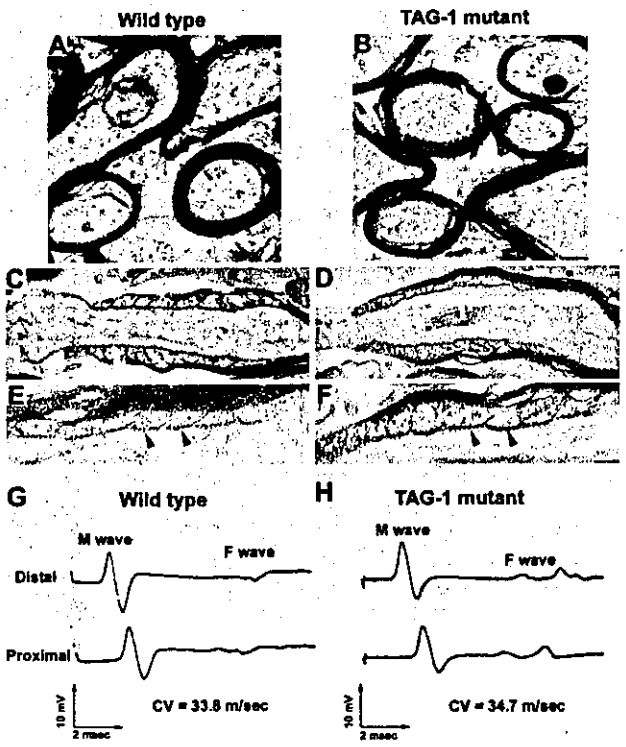

Figure 1. **Ultrastructural organization of myelinated fibers and nerve function in TAG-1 mutant mice.** (A–F) Ultrastructural organization of myelinated fibers. Myelin sheath thickness and compaction were similar in myelinated fibers of the ventral spinal cord region of 3-mo-old (A) wild-type and (B) TAG-1 mutant mice. The nodal (N), paranodal (P), and juxtaparanodal (J) regions appeared properly organized in longitudinal sections of wild-type (C) and mutant animals (D). In the paranodal region, the transverse bands (arrowheads) were normally present in both genotypes (E, wild type; F, mutant). Bars: (A and B) 0.1 μm; (C and D) 0.5 μm; and (E and F) 0.3 μm. (G and H) Electrophysiological studies of sciatic nerves. CMAPs and F waves were recorded after distal and proximal stimulation of sciatic nerves of 2-mo-old (G) wild-type and (H) TAG-1 mutant mice. There were no differences in the waveform, latencies and amplitudes of CMAPs between both genotypes.

(IF) and laser confocal microscopy in optic nerve sections of wild-type and TAG-1–deficient mice. Double labeling for sodium channels and paranodin/Caspr in wild-type (Fig. 2 A) and mutant mice (Fig. 2 B) demonstrated normal clustering of these proteins in the nodal and paranodal regions, respectively, in both genotypes. We analyzed the organization of the juxtaparanodal regions of the TAG-1 mutant optic nerves by examining the expression of Caspr2 and Kv1.1 potassium channels subunits. As expected, in wild-type animals, Caspr2 was detected at juxtaparanodes in reference to the nodal sodium channels (Fig. 2 C), whereas in mutant mice, no enrichment of Caspr2 IR was detectable (Fig. 2 D). K^+ channels distribution was also dramatically altered in mutant fibers because the overall staining for Kv1.1 was decreased and appeared to occupy much smaller areas than in wild-type animals (Fig. 2, E and F). Kv1.1-IR was detected only at the vicinity of paranodes in almost all the sites examined in the mutant optic nerves (Fig. 2 F, arrows). Similar alterations of Caspr2 and Kv1.1 channel distribution, contrasting with unchanged nodal and paranodal markers, were observed in spinal cord (unpublished data), indicating that TAG-1 plays a general role in the organization of axo–glial juxtaparanodal contacts in the CNS.

The dramatic alterations of Caspr2 and Kv1.1-IR in juxtaparanodal regions raised the possibility that TAG-1 might control either their expression levels or their enrichment in these regions. To address this question we measured the levels of these proteins by immunoblot (IB) of optic nerve extracts. In the mutants, as expected, no TAG-1 immunoreactive band was observed (Fig. 3 A), whereas Caspr2 levels were virtually unchanged (Fig. 3 B). Kv1.1 antibodies revealed a doublet (Fig. 3 C), which may correspond to the 86-kD mature,

Table I. **Parameters of compound action potentials from wild-type and TAG-1 mutant sciatic nerves**

	Units	(+/+) $n = 9$	(+/−) $n = 5$	(−/−) $n = 11$
DL	ms	1.14 ± 0.19	1.18 ± 0.15	1.17 ± 0.16
PL	ms	1.82 ± 0.18	1.78 ± 0.15	1.83 ± 0.20
CV	m/s	34.02 ± 3.64	35.64 ± 2.83	35.23 ± 3.61
AMP (D)	mV	11.51 ± 4.54	11.76 ± 3.46	14.90 ± 3.03
AMP (P)	mV	10.11 ± 3.51	10.78 ± 2.65	13.06 ± 2.99

Distal latencies (DL), proximal latencies (PL), conduction velocities (CV), distal (D), and proximal (P) CMAP amplitudes (AMP) were measured in sciatic nerves of wild-type (+/+), and heterozygous (+/−) or homozygous (−/−) mutant 2-mo-old mice.
*$P > 0.05$ ANOVA for all parameters.

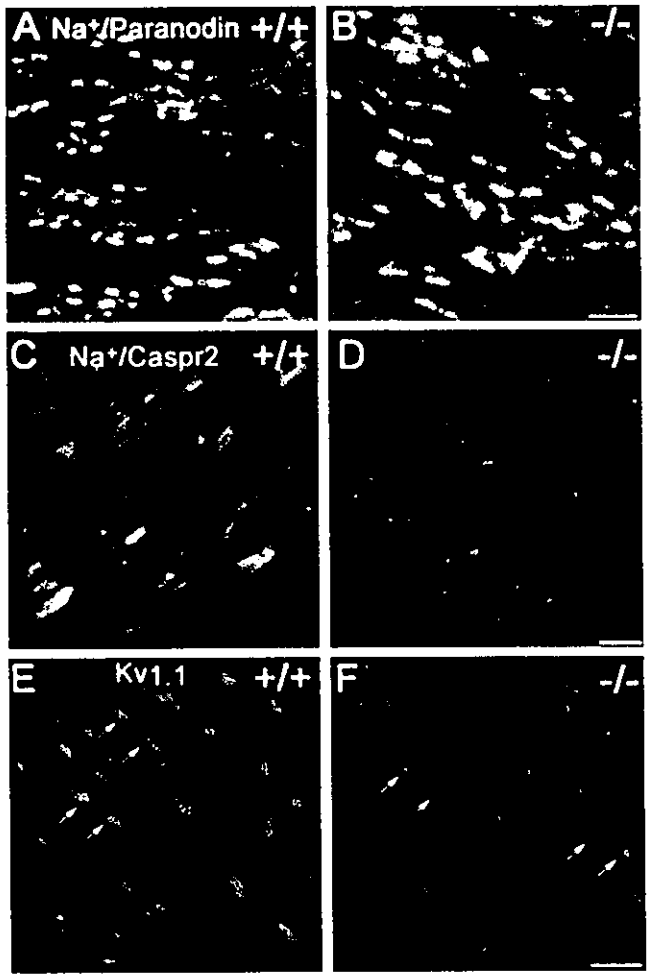

Figure 2. **Distribution of specific proteins in myelinated optic nerves of TAG-1 mutant mice.** Localization of molecular components of nodes, paranodes, and juxtaparanodes in optic nerve sections of 2-mo-old (A, C, and E) wild-type (+/+) and (B, D, and F) TAG-1 mutant (−/−) mice. Sodium channels (red) and paranodin/Caspr (green) were normally clustered in the nodal and paranodal regions, respectively, in both (A) wild-type and (B) TAG-1–deficient mice. Caspr2-IR (green) was normally detected in the juxtaparanodal regions, in reference to the nodal sodium channels (red) in (C) wild-type animals, whereas it was not visible in (D) TAG-1 mutant mice. Kv1.1-IR was dramatically altered in mutant mice (F, arrows), as compared with wild-type animals (E, arrows). In TAG-1 mutant mice, Kv1.1 labeling was markedly decreased and was mostly restricted to a small area in contact with (F) paranodes. Bars: (A–F) 5 μm.

and 70-kD immature forms of these channels (Manganas and Trimmer, 2000). In mutant mice, the lower immunoreactive band was markedly increased, whereas the upper band was not significantly altered (Fig. 3 C). Thus, the biochemical measurements demonstrated that the dramatic alterations in Caspr2 and Kv1.1 channels in TAG-1 mutant mice did not result from defects in their expression but rather from the lack of concentration of these proteins in juxtaparanodal regions, presumably below IF detection levels.

Juxtaparanodal markers are severely altered in the PNS of TAG-1 mutant mice

To determine whether TAG-1 was also critical for the molecular organization of peripheral nerve fibers, we examined the localization of markers of the nodal regions in sciatic nerves of TAG-1 knockout mice and wild-type littermates (Fig. 4). In wild-type animals, TAG-1-IR was enriched in juxtaparanodal regions, adjacent to paranodes, labeled with

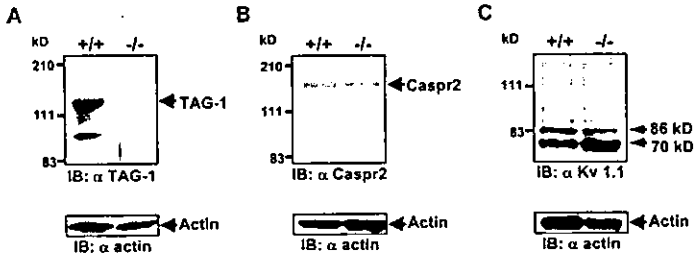

Figure 3. **Expression levels of juxtaparanodal proteins in central myelinated fibers of TAG-1 knockout mice.** Expression levels of (A) TAG-1, (B) Caspr2, and (C) Kv1.1 potassium channels in 2-mo-old wild-type (+/+) and TAG-1 mutant mice (−/−) were examined by IB analysis of optic nerve extracts (top). Protein levels were quantified (three mice in each group) using actin (bottom) in each sample for normalization: Caspr2 levels in mutant mice were 84 ± 2% of wild-type (mean ± SD); Kv1.1 86-kD band; 129± 22%; and 70-kD band 193 ± 21%. The position of molecular mass markers (kD) is indicated.

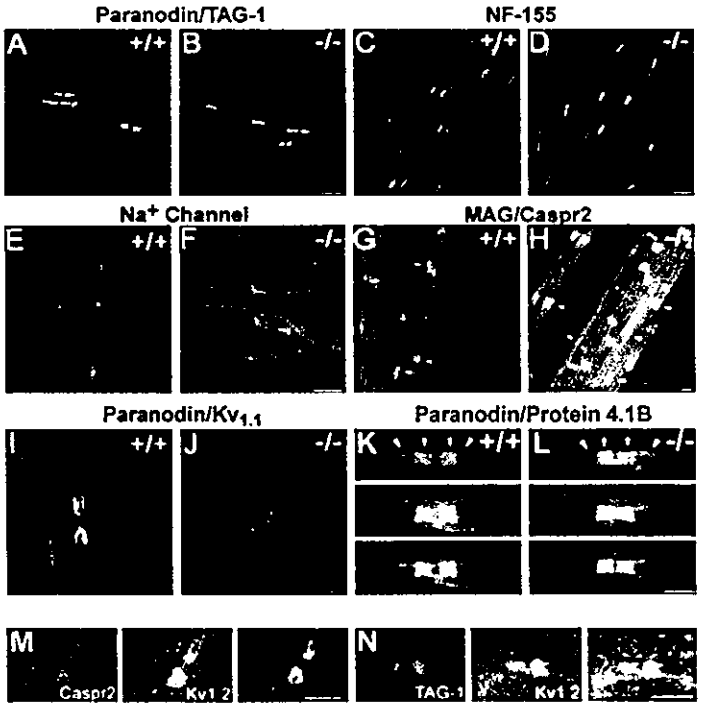

Figure 4. **Distribution of specific proteins in sciatic nerves nodal regions of TAG-1 mutants and during development.** (A–L) Localization of molecular components of nodes, paranodes, and juxtaparanodes in teased sciatic nerve fibers of 2-mo-old (A, C, E, G, I, and K) wild-type (+/+) and (B, D, F, H, J, and L) TAG-1 mutant (−/−) mice: (A and B) TAG-1 (red) and paranodin/Caspr (green); (C and D) NF155; (E and F) sodium channels; (G and H) MAG (green, paranodal regions, arrows; Schmidt-Lanterman incisures, arrowheads) and Caspr2 (red); (I and J) Kv1.1 potassium channels (green) and Caspr/paranodin (red); (K and L) Protein 4.1B (red) and Caspr/paranodin (green). Caspr2 and Kv1.1 labeling were dramatically altered in mutant mice, whereas the other markers appeared normal. Protein 4.1B-IR (red) was intense in the paranodal regions (arrows) where it was colocalized with Caspr/paranodin (green), and was also visible in the juxtaparanodal regions (arrowheads) of wild-type and mutant mice. Bars: (A–J) 20 μm and (K and L) 5 μm. (M and N) Distribution of Caspr2, TAG-1 and Kv1.2 in teased fibers of sciatic nerve of a P8 rat. (M) Caspr2 (red) and (N) TAG-1 (red) were detected in a limited number of fibers, where they appeared colocalized with (M and N) Kv1.2 potassium channels (green). Bar, 2.5 μm.

paranodin/Caspr (Fig. 4 A), as reported previously (Traka et al., 2002). In mutant mice, TAG-1-IR was absent, as expected, whereas paranodin/Caspr-IR appeared normal (Fig. 4 B). The glial protein NF155 was also properly localized at paranodes (Fig. 4, C and D) and sodium channels were normally restricted to the nodes in nerves of mice of both genotypes (Fig. 4, E and F). Myelin-associated glycoprotein (MAG) was normally enriched in paranodal regions, as well as at Schmidt-Lanterman incisures in wild-type and TAG-1 mutant mice (Fig. 4, G and H). Thus, in the absence of TAG-1, the major nodal and paranodal proteins were normally localized in sciatic nerves.

In contrast, the molecular organization of the juxtaparanodal regions of the TAG-1 mutant sciatic nerves was severely altered. We were unable to detect localized Caspr2 labeling in the mutants compared with wild-type mice (Fig. 4, G and H), and a dramatic reduction of the Kv1.1-IR was observed in TAG-1–deficient mice (Fig. 4, I and J). Similar results were obtained for Kv1.2 (unpublished data). Quantitative analysis of Kv1.1 and Kv1.2 channel distribution in mutant sciatic nerve fibers showed all the nodal sites to be affected: 417 nodes from four mice were analyzed for Kv1.1, and 233 nodes from two mice for Kv1.2; K^+ channels accumulation was undetectable in 70% of the mutant juxtaparanodes examined, whereas a reduced clustering, as in Fig. 4 J, was observed in the rest of the sites. IB analysis showed that Caspr2 protein levels were unchanged in TAG-1 mutant sciatic nerves (106 ± 22% of wild type, mean ± SD, $n = 3$), whereas the levels of the immature band of Kv1.1 was increased (194 ± 40% of wild-type levels, mean ± SD, $n = 3$). Thus, the dramatic alteration of Caspr2 and K^+ channels enrichment in the absence of TAG-1, demonstrated their failure to accumulate in juxtaparanodal regions of peripheral myelinated fibers and not an expression defect.

Protein 4.1B is enriched at paranodes and, to a lesser degree, at juxtaparanodes (Ohara et al., 2000), where it interacts with the intracellular domain of Caspr/paranodin and Caspr2, respectively (Gollan et al., 2002; Denisenko-Nehrbass et al., 2003b). We examined the localization of protein 4.1B in TAG-1 mutants (Fig. 4, K and L). In wild-type mice protein 4.1B-IR was highly concentrated at paranodes (Fig. 4 K, arrows) and was also present at juxtaparanodes (Fig. 4 K, arrowheads). In TAG-1–deficient mice the localization of protein 4.1B at paranodes was unchanged, whereas only a small decrease was observed at juxtaparanodes (Fig. 4 L). Quantification in three wild-type and four mutant nerves revealed that the proportion of juxtaparanodes where 4.1B-IR was clearly visible, was 92 ± 1% and 70 ± 3%, respectively (mean ± SEM, $P < 0.01$, t test). Altogether these observations demonstrated that in the absence of TAG-1 the juxtaparanodal enrichment of Caspr2 was lost and that of K^+ channels was severely disrupted. In contrast, protein 4.1B was only moderately affected, indicating that its juxtaparanodal localization is largely independent of the presence of Caspr2.

TAG-1, Caspr2, and K^+ channels are colocalized early during myelination

Because our data indicated a role of TAG-1 in the targeting of Caspr2 and K^+ channels, it was important to determine whether these three proteins were found at the same

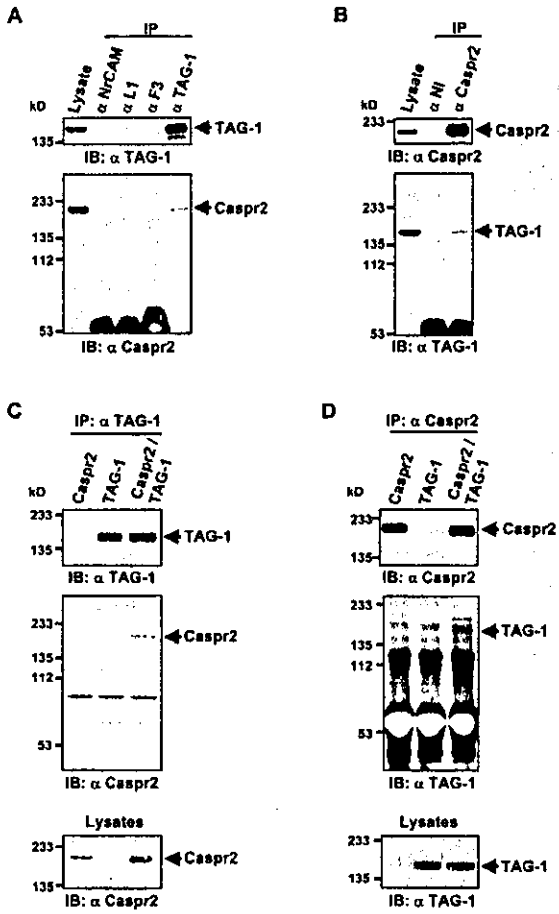

Figure 5. **Association of TAG-1 and Caspr2 in brain and transfected COS-7 cells.** (A and B) Association of TAG-1 and Caspr2 in brain. Rat brain proteins were extracted and subjected to IP with (A) αCaspr2 or (B) αTAG-1. The presence of specific proteins in the precipitates was examined by IB with the indicated antibodies. Aliquots of crude protein extracts (Lysate, 1/60 of protein amount used for each coIP) were also subjected to IB to verify the expression of the proteins. (A) Caspr2 was detected in immune precipitates with TAG-1 antibodies but not with antibodies against other IgSF proteins (αNrCAM, αL1, and αF3). (B) TAG-1 was detected in immune precipitates with Caspr2 antibodies but not nonimmune serum (αNI). (C and D) Association of TAG-1 and Caspr2 in transfected COS-7 cells. Lysates from COS-7 cells overexpressing either Caspr2 or TAG-1 alone, or both, were prepared as described in Materials and methods and subjected to IP either with (C) αTAG-1 or (D) αCaspr2. Precipitates were resolved by SDS-PAGE, analyzed by IBs with antibodies against Caspr2 and TAG-1, to detect the presence of specific proteins (C and D, top and middle). Aliquots of crude protein extracts (Lysates) were also subjected to immunoblotting to verify the expression of the proteins (C and D, lower panels). TAG-1 antibodies coIP Caspr2 only in doubly transfected cells (C), whereas Caspr2 antibodies pulled-down TAG-1 only in cotransfected cells (D). Note the slight shift of migration of Caspr2 in the presence of TAG-1, which results in a doublet with a predominant lower band in cotransfected cells (C, Lysates). The position of molecular mass markers (kD) is indicated.

locations early during development. We examined the localization of TAG-1, Caspr2, and Kv1.2 in rat sciatic nerve at postnatal day 8 (P8), a time around which K^+ channels appear in a few fibers, transiently localized at nodes and paranodes, and then progressively to the juxtaparanodes (Vabnick et al., 1999), whereas Caspr2 has been reported to follow K^+ channel distribution (Poliak et al., 2001). At P8, localized enrichment of these proteins was detected in a limited number of fibers (Fig. 4, M and N). We confirmed the colocalization of Caspr2 and Kv1.2 (Fig. 4 M), and we found that TAG-1-IR always overlapped with Kv1.2-IR (Fig. 4 N). These results indicate that TAG-1 is colocalized with Caspr2 and Kv1.2 channels early during development, and support its involvement in the targeting of these proteins.

TAG-1 and Caspr2 are associated in brain and in transfected cells

The colocalization of TAG-1 and Caspr2 in mice and rats, together with the mislocalization of Caspr2 in TAG-1–deficient mice prompted us to examine the possibility that these proteins form a complex at juxtaparanodes by performing coimmunoprecipitation experiments from brain extracts. Caspr2 was detected in TAG-1 immune precipitates but not in immunoprecipitation (IP) performed with antibodies against other IgSF proteins (Fig. 5 A). Conversely, TAG-1 was specifically detected in Caspr2 immune precipitates (Fig. 5 B). These results indicate the existence of a specific association between TAG-1 and Caspr2 in vivo. We examined further the association between TAG-1 and Caspr2 using COS-7 cells transfected with expression plasmids for either of these proteins, alone or in combination (Fig. 5, C and D). IP with TAG-1 antibodies pulled down Caspr2 in cells doubly transfected with TAG-1 and Caspr2 but not in cells expressing only Caspr2 (Fig. 5 C). On the other hand, Caspr2 antibodies coprecipitated TAG-1 only in doubly transfected cells (Fig. 5 D).

TAG-1 and Caspr2 form a cis complex at the plasma membrane

We investigated whether the association of TAG-1 and Caspr2 altered their subcellular localization in transfected COS-7 cells. When transfected alone, Caspr2 or TAG-1 were, for the most part, localized at the level of the plasma membrane (Fig. 6, A and B). However, the IR pattern of these two proteins was different because Caspr2 appeared rather uniformly distributed, whereas TAG-1-IR had a punctate or patchy appearance, as reported previously in transfected CHO cells (Buttiglione et al., 1998). When both proteins were simultaneously expressed, they were largely colocalized at the plasma membrane, and their distribution appeared similar to that of Caspr2 alone (Fig. 6 C).

TAG-1 is a GPI-anchored protein found in cholesterol-rich, Triton X-100–insoluble membrane fractions (Buttiglione et al., 1998; Kasahara et al., 2000; Prinetti et al., 2001). In transfected COS-7 cells, TAG-1 was Triton X-100 insoluble at 4°C, whereas Caspr2, a type 1 transmembrane protein, was soluble (unpublished data). We examined the

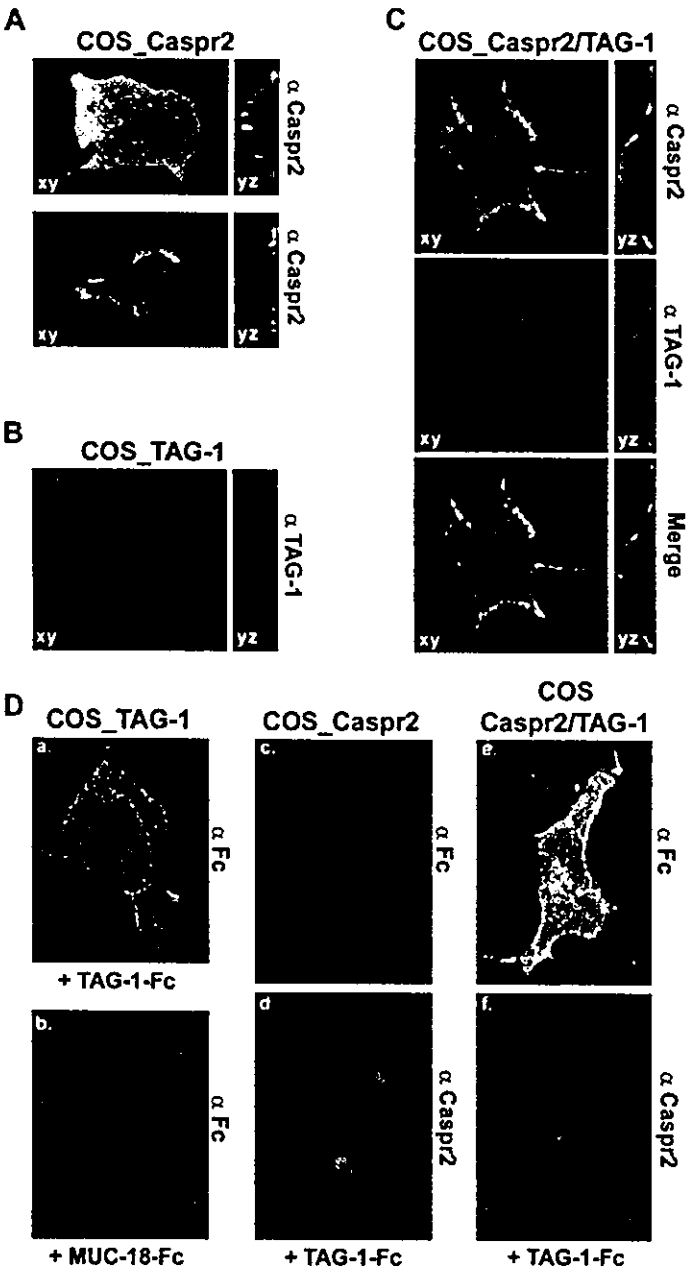

Figure 6. **Cis and trans interactions between TAG-1 and Caspr2 in COS-7 cells.** (A–C) Colocalization of Caspr2 and TAG-1 at the plasma membrane of COS-7 cells. COS-7 cells overexpressing either Caspr2 or TAG-1 alone, or both, were processed for indirect IF and laser confocal microscopy analysis. Caspr2 was uniformly localized at the plasma membrane (A, COS_Caspr2). TAG-1 displayed a membrane localization with a patchy appearance (B, COS_TAG-1). In cotransfected cells, Caspr2 (green) and TAG-1 (red) were largely colocalized (yellow) at the plasma membrane with a distribution similar to that of Caspr2 alone (C, COS_Caspr2/TAG-1). Single confocal sections are shown. (D) Association of TAG-1 in trans with itself but not with Caspr2. COS-7 cells overexpressing either TAG-1 alone (COS_TAG-1, a and b), Caspr2 (COS_Caspr2, c and d) or both (COS_Caspr2/TAG-1, e and f) were incubated with a (a and c–f) TAG-1-Fc chimeric protein or a (b) MUC-18-Fc chimera protein, and processed for indirect IF and laser confocal microscopy analysis. The TAG-1-Fc chimeric protein (green) bound to cells expressing (a) TAG-1 alone or in combination with (e) Caspr2 but not to cells expressing (c) Caspr2 alone. Expression of Caspr2 was verified by (d and f) specific IF (red). Stacked confocal images of eight consecutive sections 1 μm apart. Bar, (A–D) 10 μm.

membrane compartments in which Caspr2 and TAG-1 were distributed and whether their coexpression altered this distribution by loading Triton X-100 cell lysates on discontinuous sucrose gradients (Fig. 7). Analysis of the proteins in the fractions revealed that TAG-1 was present in the 10 and 25% sucrose fractions (Fig. 7 A, top). In contrast, Caspr2 expressed alone was recovered in the heavier 40% fraction and in the pellet (Fig. 7 B, top). When coexpressed with Caspr2, TAG-1 was no longer present in the light fractions but was only found in the pellet with Caspr2 (Fig. 7, A and B, bottom). These experiments indicate that when Caspr2 and TAG-1 are coexpressed, their interaction alters the distribution of TAG-1 by changing its microenvironment and/or by linking the complexes to cytoplasmic components. Altogether our results reveal that Caspr2 is able to reach the plasma membrane by itself, and that Caspr2 and TAG-1 are colocalized and associated in cis at the plasma membrane in transfected cells.

TAG-1 associates in trans with itself but not with Caspr2

The results reported above underline the ability of TAG-1 to associate with Caspr2 in the same membrane. However, TAG-1 is also highly expressed in myelinating glial cells and its enrichment in juxtaparanodes is likely to result, at least in part, from its accumulation in the glial membrane (Traka et al., 2002). This localization suggested that TAG-1 could interact with the TAG-1–Caspr2 complex in the facing axolemma. To examine the possibility of such trans interactions, we incubated COS-7 cells expressing TAG-1 and/or Caspr2 with a TAG-1-Fc chimeric protein (Fig. 6 D). TAG-1-Fc was readily capable to interact with cells transfected with TAG-1 (Fig. 6 D), confirming its well-characterized homophilic recognition properties (Tsiotra et al., 1996; Pavlou et al., 2002). The specificity of the interaction was indicated by the lack of binding of a MUC-18-Fc chimera to these cells (Fig. 6 D, b). The TAG-1-Fc chimeric protein did not bind to cells transfected with Caspr2 alone (Fig. 6 D, c and d), whereas it interacted with cells cotransfected with Caspr2 and TAG-1 (Fig. 6 D, e and f). The binding of TAG-1-Fc to cells expressing only TAG-1 or TAG-1 and Caspr2 appeared similar. These results show that TAG-1 was not able to interact in trans with Caspr2, but that the presence of Caspr2 did not alter the capacity of TAG-1 to establish trans homophilic interactions.

Discussion

Axo–glial interactions result in a highly segregated distribution of membrane proteins, defining distinct domains of the axolemma. The mechanisms leading to the enrichment of Na^+ channels and associated proteins at the nodes of Ranvier, as well as those involved in the formation of paranodal axo–glial junctions, have been extensively investigated (for review see Girault and Peles, 2002). In contrast, hardly anything is known about the basis for the accumulation of specific proteins, including potassium channels, at juxtaparanodes. The present work demonstrates the critical role of TAG-1 for the enrichment of axonal proteins Caspr2 and Kv1.1/Kv1.2 in juxtaparanodal regions, and points out unexpected molecular similarities in axo–glial interactions at paranodes and juxtaparanodes.

Despite the lack of major ultrastructural or functional alterations of myelinated fibers in TAG-1–deficient mice, a detailed analysis revealed that the normal distribution of the known molecular components of the juxtaparanodal region was selectively disturbed in the CNS and PNS of these animals. Although the localization of Na^+ channels and paranodal proteins was normal in TAG-1 mutant mice, the normal accumulation of Caspr2 at juxtaparanodes was completely lost and the distribution of delayed rectifier K^+ channels was severely altered. Thus, the phenotype of TAG-1–deficient mice is markedly different from that of other mutant strains described so far. For example, deletion of oligodendrocytes in transgenic mice during the first days after birth induces a virtually complete absence of organization of axonal proteins beyond the initial segments (Mathis et al., 2001). Dysmyelination in *jimpy* mice or *md* rats, as well as targeted mutations in the galactolipid biosynthetic pathway, severely alter the organization of paranodal junctions without preventing the initial accumulation of K^+ channels in direct contact with the nodes (Dupree et al., 1999; Mathis et al., 2001, Arroyo et al., 2002). Targeted mutations of paranodal proteins prevent the formation of septate-like junctions and also result in a lack of separation between K^+ channels and Na^+ channels clusters (Bhat et al., 2001; Boyle et al., 2001). These observations support a role of fence for the paranodal junction (Pedraza et al., 2001), separating the internode from the node. They also strongly indicate that the mechanisms leading to the accumulation of K^+ channels and Caspr2 in the juxtaparanodal regions are relatively independent from those governing the formation of nodes and paranodal junctions. Thus, the phenotype of TAG-1 mutants provides novel insights into the organization of axonal domains.

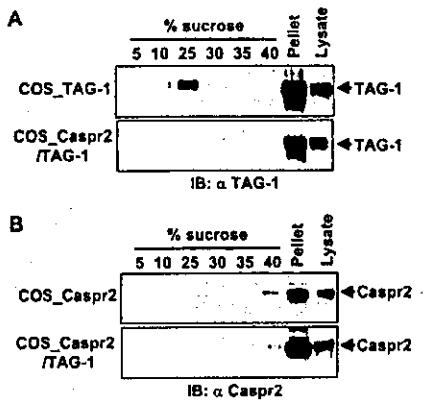

Figure 7. **Sucrose density gradient of TAG-1 and Caspr2 in transfected COS-7 cells.** COS-7 cells overexpressing either (A, top, COS_TAG-1) TAG-1 alone or (B, top, COS_Caspr2) Caspr2 alone, or (A and B, bottom, COS_Caspr2/TAG-1) both proteins, were lysed in a Triton X-100 containing buffer and lysates were submitted to discontinuous sucrose gradients as described in Materials and methods and IB with antibodies against (A) TAG-1 and (B) Caspr2. Aliquots of crude protein extracts (Lysate) were also analyzed to verify the expression of the proteins. TAG-1 expressed alone was present in the 10 and 25% sucrose fractions (A, top). In contrast, Caspr2 was recovered in the heavier 40% fraction and in the pellet (B, bottom). When coexpressed with Caspr2, TAG-1 was no longer present in the light fractions but was found in the pellet with Caspr2 (A and B, bottom).

Our results show that TAG-1 is closely associated with Caspr2 and is required for its accumulation at juxtaparanodes by recruiting and/or stabilizing it at this location. Co-IP experiments demonstrated that Caspr2 and TAG-1 form a complex in brain and in transfected cells. In addition, the two proteins were colocalized at the plasma membrane, and the presence of Caspr2 modified TAG-1 membrane distribution, which became more diffuse in intact cells and disappeared from the light fractions in sucrose gradients. These results indicate that the association of the two proteins alters significantly their membrane microenvironment and/or their interaction with other proteins.

Our findings in COS-7 cells demonstrate that TAG-1 can exchange cis interactions with Caspr2. This ability supports an association between the two proteins in the axolemma be-

cause TAG-1 is expressed in several types of neurons (Dodd et al., 1988; Karagogeos et al., 1991), including adult neurons of the dorsal root ganglia and their projections (unpublished data) and spinal motor neurons (Traka et al., 2002). However, TAG-1 is also expressed in Schwann cells and oligodendrocytes and could be expected to exchange trans interactions with Caspr2. We tested this possibility using TAG-1-Fc chimeras and did not observe any binding, suggesting that in these conditions the two proteins interact directly only if they are present in the same membrane, in the same orientation. Yet, in these assays, TAG-1-Fc was readily capable to bind to membrane-bound TAG-1, in the absence or presence of cotransfected Caspr2. Thus, our results are compatible with a model in which TAG-1 interacts in cis with Caspr2 in the axolemma and in trans, through homophilic interaction, with another molecule of TAG-1 in the glial membrane (Fig. 8). A precedent for this type of interaction has been shown to occur between TAG-1 and L1 (Malhotra et al., 1998). In that case, the trans homophilic interaction between TAG-1 molecules resulted in cis activation of L1, inducing its binding to ankyrin. Although the model depicted in Fig. 8 is the simplest that accounts for all the presently available data, the possibility that additional components are part of this macromolecular complex cannot be excluded, as TAG-1 has been shown to interact with several other extracellular proteins (Milev et al., 1996; Pavlou et al., 2002). In addition, the association of Caspr2 with protein 4.1B (Denisenko-Nehrbass et al., 2003b) suggests that the TAG-1–Caspr2 ternary complexes may be attached to the cytoskeleton through this protein that has the capability to interact with actin and spectrin (Gimm et al., 2002). In TAG-1 knockout mice, we found that protein 4.1B was still present in juxtaparanodal regions although Caspr2-IR was not accumulated in these regions. This observation indicates that additional targeting mechanisms account for the localization of protein 4.1B to juxtaparanodes, and that the presence of protein 4.1B is not sufficient to induce the accumulation of Caspr2 in these regions. Therefore, we suggest that the combination of two complementary mechanisms may be required for the normal localization of the TAG-1–Caspr2 ternary complexes at juxtaparanodes: an axo–glial, TAG-1–mediated, homophilic interaction, and the anchoring of Caspr2 to cytoskeletal elements in the axon that may be found only in the vicinity of nodes of Ranvier. A prediction of this model is that TAG-1 localization should be altered in the absence of Caspr2 or of protein 4.1B.

An important conclusion of this paper is that TAG-1 is also essential for K^+ channels enrichment at juxtaparanodes because a severely disrupted distribution of Kv1.1 and Kv1.2 was observed in mutant mice. It should be pointed out that the normal basic electrophysiological properties of TAG-1–deficient sciatic nerves is not surprising given the known insensitivity of adult sciatic nerves to K^+ channel blockers (Vabnick et al., 1999) and the absence of dysmyelination in TAG-1 mutants (this paper). Further analysis of TAG-1–deficient mice might be useful to address the function of the juxtaparanodal K^+ channels. At any rate, this paper provides insights into the mechanisms of enrichment of these channels. These channels can coprecipitate with Caspr2 and there is indirect evidence that PDZ domain proteins are necessary for this association (Poliak et al., 1999; Rasband et al., 2002; Fig. 8). Alternatively, the accumulation of K^+ channels could originate from their interaction with TAG-1, a possibility that remains to be formally ruled out. Interestingly, some K^+ channel accumulation was still observed in the vicinity of paranodes of 2-mo-old TAG-1–deficient mice in the absence of detectable Caspr2, indicating the minor contribution of additional targeting mechanism(s).

Paranodin/Caspr and contactin/F3, are essential for the formation of septate junctions where their glial partner is NF155, a transmembrane IgSF. Moreover, neurexin IV, the *Drosophila* member of the NCP family is essential for septate junction formation in flies (Baumgartner et al., 1996) and may form a tripartite complex with D-contactin and neuroglian, the orthologues of contactin/F3 and NF155, respectively (Faivre-Sarrailh, C., and M. Bhat, personal communication). Therefore, a core tripartite complex encompassing a NCP and a contactin-like protein in one membrane and an IgSF protein in the facing membrane appears to be a conserved molecular building block of intercellular contacts.

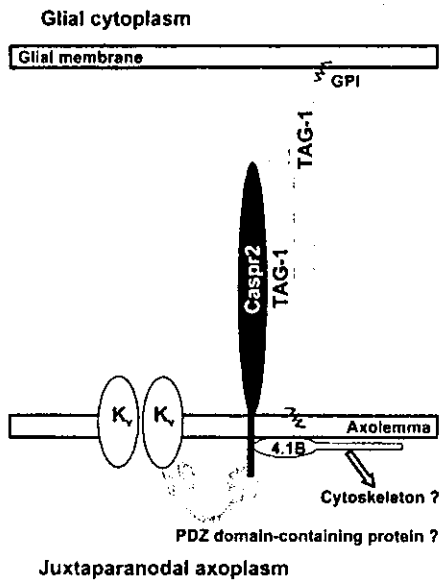

Figure 8. **Model of the molecular organization of juxtaparanodal regions.** This model is the simplest that can account for the data from previous studies and the present work. Caspr2 is enriched in the axolemma, whereas TAG-1 is expressed in both neurons and myelinating glial cells. Experiments in transfected cells show that TAG-1 interacts with Caspr2 in cis, and that TAG-1 exchanges trans interactions with itself (homophilic) but not with Caspr2. The functional importance of these interactions is demonstrated by the absence of Caspr2 enrichment in juxtaparanodal regions in TAG-1 knockout mice. These complexes are associated with other proteins including Kv1.1 and Kv1.2 potassium channels, presumably through a PDZ domain–containing protein (schematically represented here; Poliak et al., 1999; Rasband et al., 2002) and with protein 4.1B (Denisenko-Nehrbass et al., 2003b). Because protein 4.1B was still detected at juxtaparanodes in the absence of TAG-1 and Caspr2, it is likely that it interacts with other proteins, including components of the cytoskeleton (arrow). Correct localization of juxtaparanodal proteins may depend on both axo–glial interactions and binding to axoplasmic cytoskeletal components.

The latter IgSF protein can be a transmembrane protein in the case of paranodal septate-like junctions and *Drosophila* septate junctions, or a contactin-like molecule in the case of juxtaparanodes (this paper).

The molecular similarities between paranodal and juxtaparanodal protein complexes contrast with the striking ultrastructural differences between these two regions. At paranodes, the plasma membranes are separated by a narrow gap, interrupted by regularly spaced electron dense material that forms septa, in register with regularly organized intramembrane particles in glial and axonal membranes, as detected by freeze fracture (Wiley and Ellisman, 1980). In contrast, at juxtaparanodes the membranes are more loosely apposed and do not display septate-like junctions. Freeze fracture has only revealed the presence of sparse particles in juxtaparanodal axonal and glial membranes (Stolinski et al., 1981; Tao-Cheng and Rosenbluth, 1984), which may correspond to ion channels and, possibly, to Cx 29 hemichannels (Stolinski et al., 1981; Tao-Cheng and Rosenbluth, 1984; Li et al., 2002). Thus, the conserved NCP–IgSF ternary complexes appear to be involved in strikingly distinct types of cell–cell contacts. A noticeable difference is that NF155, the glial moiety of this complex at paranodes, is a transmembrane protein, presumably associated with the cytoskeleton, as in *Drosophila* septate junctions, whereas at juxtaparanodes, TAG-1 is a GPI-anchored protein. Further experiments will be required to determine whether this difference accounts for the striking differences between paranodal and juxtaparanodal NCP-contactin–based intercellular complexes, or whether additional components are involved. In either case, the present work demonstrates the contribution of TAG-1 and associated Caspr2 in the organization of axonal domains at nodes of Ranvier.

Materials and methods

Mice

TAG-1 knockout mice were produced as described previously (Fukamauchi et al., 2001) and kept as heterozygote breeding pairs. The housing and animal procedures used were in agreement with European Union policy.

Standard EM

Two wild-type mice and two mutant littermates were deeply anesthetized by Avertin (0.425 mg/g; i.p.), perfused transcardially with 2% PFA/2.5% glutaraldehyde in 0.1 M cacodylate buffer, pH 7.4, containing 1 mM $CaCl_2$. The spinal cords were immersed in the fixative for 2 h at RT. Samples were rinsed in 0.1 M cacodylate buffer containing 4% sucrose and fixed after in 2% OsO_4, rinsed, and dehydrated in an ascending series of ethanol. The samples were embedded flat in a mixture of Epon and Araldite. Ultra-thin sections were stained with uranyl acetate and lead citrate and were examined with an electron microscope (model EM 201C; Philips).

Electrophysiological studies

Studies were performed on sciatic nerves of mice anesthetized with Avertin (0.5 mg/g; i.p.) with temperature maintained at 31°C. Recording needle electrodes were placed subcutaneously in the footpad. Supramaximal stimulation of sciatic nerves was performed with a 0.1–0.2 ms rectangular pulse, stimulating distally at the ankle and proximally at the sciatic notch with needle electrodes. Recordings were obtained on a TECA Neurostar (Oxford Instruments) with a filter setting of 2 Hz to 10 kHz. Latencies correspond to the time lapse between the stimulus and the onset of CMAPs. Conduction velocities were calculated as follows: conduction velocities = distance /(proximal latency − distal latency). The peak to peak amplitudes of CMAPs were measured and the ratio of proximal versus distal amplitude was used to determine the presence or absence of partial conduction block.

Antibodies and constructs

The mAb 1C12 against TAG-1 was used for IP and IF of transfected cells, whereas polyclonal antibodies for immunostaining of teased fibers and IBs were used (Dodd et al., 1988; Traka et al., 2002). Polyclonal antisera against paranodin/Caspr (L-51) and Caspr2 have been described previously (Menegoz et al., 1997; Denisenko-Nehrbass et al., 2003b). mAbs against MAG (Poltorak et al., 1987), and Caspr (Poliak et al., 1999), and the polyclonal antibodies against NF155 (Tait et al., 2000), F3, NrCAM, and L1 were provided by M. Schachner (Zentrum für Moleculare Neurobiologie, Hamburg, Germany), E. Peles (The Weizmann Institute, Rehovot, Israel), P. Brophy (University of Edinburgh, Edinburgh, UK), C. Faivre-Sarrailh (Institute of Jean Roche, Marseille, France), and T. Galli (UMPC, Paris, France). The sodium channel (PAN) mAb was purchased from Sigma-Aldrich; Kv1.1 and Kv1.2 mAbs were purchased from Upstate Biotechnology; actin mAb was purchased from Amersham Biosciences; polyclonal anti–human Fc, goat anti–rabbit Cy3, and goat anti–mouse Cy3 antibodies were purchased from Jackson ImmunoResearch Laboratories; and goat anti–rabbit Alexa Fluor 488, anti–mouse Alexa Fluor 488, and anti–mouse Alexa Fluor 594 antibodies were purchased from Molecular Probes. HRP-conjugated goat anti–mouse and anti–rabbit antibodies used for immunoblotting were purchased from Amersham Biosciences.

For expression of TAG-1 in COS-7 cells, Pc-TAG consisting of the entire coding region of rat TAG-1 cloned in the pcDNA1 vector (Invitrogen; Buttiglione et al., 1998) was used. The human Caspr2 cDNA (NM_014141, KIAA0868), provided by O. Ohara (Kazusa DNA Research Institute, Kisarazu, Japan), was introduced into the KpnI/NotI sites of the pcDNA3 vector (Invitrogen). Production of TAG-1-Fc (human homologue of rat TAG-1 fused to the Fc region of the human IgG1) and MUC-18-Fc was as described previously (Buttiglione et al., 1998; Pavlou et al., 2002). In the transient transfection experiments to detect Fc binding, the human homologue of TAG-1 cloned in the pcDNA3 vector was used (Pavlou et al., 2002).

Immunohistofluorescence

Sciatic and optic nerves from adult wild-type and mutant animals, as well as sciatic nerves from P8 rats, were dissected and fixed in 2% PFA for 30 min at RT. Sciatic nerves were teased apart to yield single fiber preparations, air dried overnight at RT, and kept at −80°C. For immunostaining, teased nerve fibers, and optic nerve, 10–12 μm frozen sections were used. All tissue samples were incubated in −20°C acetone for 10 min. Specimens were further processed as described in Traka et al. (2002). Images were acquired by a laser scanning microscope (model SP; Leica) using a 40 or 63× oil objective.

Biochemical experiments

Specific protein levels in sciatic and optic nerves were performed as described previously and normalized to actin levels (Traka et al., 2002). IPs from 6 mg protein /IP of brain extracts and 1 mg/IP of transfected COS-7 cells were performed essentially as described previously (Denisenko-Nehrbass et al., 2003a), except that the extraction buffer contained 85 mM Tris, pH 7.5, 30 mM NaCl, 1 mM EDTA, 120 mM glucose, 1% Triton X-100, 60 mM *n*-octylglucoside, and 1 mM PMSF. Isolation of low density Triton X-100–insoluble complexes from transfected COS-7 cells was performed as described previously (Buttiglione et al., 1998) except that the sucrose gradient was discontinuous. Proteins of interest were detected by IB and ECL chemiluminescent detection (Amersham Biosciences).

Cell culture, IF, and Fc-binding procedures

COS-7 cells were transfected using Polyethylenimine or Fugene 6 (Roche) using 8 μg of plasmid/10-mm-diam dish and 1–2 μg of plasmid/35-mm-diam dish. After transfection, cells were grown for 24 h before processing. For TAG-1 detection, indirect labeling was performed on living cells washed once with PBS, incubated with mAb 1C12 diluted in PBS/1% BSA for 30 min at RT, washed twice with PBS, and incubated with the goat anti–mouse Alexa Fluor 594 for 30 min at RT. For Caspr2 detection, cells immunostained for TAG-1 were fixed for 20 min in 4% PFA, permeabilized with 0.02% Triton X-100 for 5 min, and incubated with the anti-Caspr2 antibody and goat anti–rabbit Alexa Fluor 488 for 30 min each at RT. Coverslips were mounted in Vectashield. For binding assays on TAG-1 or Caspr2 transfected COS-7 cells, TAG-1-Fc and MUC-18-Fc Fc-chimeras (15 μg/ml of each) were cross-linked with anti–human Fc antibody (50 μg/ml) for 1 h at 37°C and incubated as described previously (Buttiglione et al., 1998; Pavlou et al., 2002). Detection of the binding was achieved after fixation and permeabilization with anti–rabbit Alexa Fluor 488 antibody. Caspr2 was detected with polyclonal antibody and anti–rabbit Cy3 antibody. Cells were mounted in Mowiol (Calbiochem) and the images were acquired using a laser scanning microscope (model SP; Leica).

We are grateful to Drs. Brophy, Ohara, Peles, Schachner, Faivre-Sarrailh, and Galli for providing reagents and Dr. Isidoridou (Neurobiology Research Institute, Cozzika Foundation) for the EM facility; to Dr. Brian Popko for constructive comments throughout the course of this work; and to Drs. Popko and Strigini for comments on the manuscript. We thank M. Mouratidou, M. Carnaud, and K. Ogulevetskaia for their help at the final stages of this work and N. Campbell for her excellent technical assistance.

This work was supported by grants from the National Society for Multiple Sclerosis [RG3368], the IMBB, the Onassis Foundation, and the Greek Ministry of Education [EPEAEK 1092] (to D. Karagogeos); Fondation Schlumberger pour l'Education et la Recherche, Association Française contre les Myopathies, and Fondation pour la Recherche Médicale (to J.A. Girault); and National Institutes of Health RO1 NS39346-01, a gift from M.P. Miller through the Brain Research Foundation, and the Jack Miller Neuropathy Center (to B. Soliven).

Submitted: 15 May 2003
Accepted: 28 July 2003

References

Arroyo, E.J., T. Xu, J. Grinspan, S. Lambert, S.R. Levinson, P.J. Brophy, E. Peles, and S.S. Scherer. 2002. Genetic dysmyelination alters the molecular architecture of the nodal region. *J. Neurosci.* 22:1726–1737.

Baumgartner, S., J.T. Littleton, K. Broadie, M.A. Bhat, R. Harbecke, J.A. Lengyel, R. Chiquet-Ehrisman, A. Prokop, and H.J. Bellen. 1996. A *Drosophila* neurexin is required for septate junction and blood-nerve barrier formation and function. *Cell.* 87:1059–1068.

Bhat, M.A., J.C. Rios, Y. Lu, G.P. Garci-Fresco, W. Ching, M. St Martin, J. Li, and S. Einheber. 2001. Axon-glia interactions and the domain organization of myelinated axons requires neurexin IV/Caspr/Paranodin. *Neuron.* 30: 369–383.

Boyle, M.E., E.O. Berglund, K.K. Murai, L. Weber, E. Peles, and B. Ranscht. 2001. Contactin orchestrates assembly of the septate-like junctions at the paranode in myelinated peripheral nerve. *Neuron.* 30:385–397.

Buttiglione, M., J.M. Revest, O. Pavlou, D. Karagogeos, A. Furley, G. Rougon, and C. Faivre-Sarrailh. 1998. A functional interaction between the neuronal adhesion molecules TAG-1 and F3 modulates neurite outgrowth and fasciculation of cerebellar granule cells. *J. Neurosci.* 18:6853–6870.

Charles, P., S. Tait, C. Faivre-Sarrailh, G. Barbin, F. Gunn-Moore, N. Denisenko-Nehrbass, A.M. Guennoc, J.A. Girault, P.J. Brophy, and C. Lubetzki. 2002. Neurofascin is a glial receptor for the paranodin/Caspr-contactin axonal complex at the axoglial junction. *Curr. Biol.* 12:217–220.

Denisenko-Nehrbass, N., L. Goutebroze, T. Galvez, C. Bonnon, B. Stankoff, P. Ezan, M. Giovannini, C. Faivre-Sarrailh, and J.A. Girault. 2003a. Association of Caspr/paranodin with tumor suppressor schwannomin/merlin and beta-1 integrin in the CNS. *J. Neurochem.* 84:209–221.

Denisenko-Nehrbass, N., K. Oguievetskaia, L. Goutebroze, T. Galvez, Y. Yamakawa, O. Ohara, M. Carnaud, and J.A. Girault. 2003b. Protein 4.1B associates with both Caspr/paranodin and Caspr2 at paranodes and juxtaparanodes of myelinated fibers. *Eur. J. Neurosci.* 17:411–416.

Dodd, J., S.B. Morton, D. Karagogeos, M. Yamamoto, and T.M. Jessell. 1988. Spatial regulation of axonal glycoprotein expression on subsets of embryonic spinal neurons. *Neuron.* 1:105–116.

Dupree, J.L., J.A. Girault, and B. Popko. 1999. Axo–glial interactions regulate the localization of axonal paranodal proteins. *J. Cell Biol.* 147:1145–1152.

Einheber, S., G. Zanazzi, W. Ching, S. Scherer, T.A. Milner, E. Peles, and J.L. Salzer. 1997. The axonal membrane protein Caspr, a homologue of neurexin IV, is a component of the septate-like paranodal junctions that assemble during myelination. *J. Cell Biol.* 139:1495–1506.

Faivre-Sarrailh, C., F. Gauthier, N. Denisenko-Nehrbass, A. Le Bivic, G. Rougon, and J. Girault. 2000. The GPI-anchored adhesion molecule F3/contactin is required for surface transport of paranodin/caspr. *J. Cell Biol.* 149:491–502.

Fukamauchi, F., O. Aihara, Y.J. Wang, K. Akasaka, Y. Takeda, M. Horie, H. Kawano, K. Sudo, M. Asano, K. Watanabe, and Y. Iwakura. 2001. TAG-1-deficient mice have marked elevation of adenosine A1 receptors in the hippocampus. *Biochem. Biophys. Res. Commun.* 281:220–226.

Furley, A.J., S.B. Morton, D. Manalo, D. Karagogeos, J. Dodd, and T.M. Jessell. 1990. The axonal glycoprotein TAG-1 is an immunoglobulin superfamily member with neurite outgrowth-promoting activity. *Cell.* 61:157–170.

Gimm, J.A., X. An, W. Nunomura, and N. Mohandas. 2002. Functional characterization of spectrin-actin-binding domains in 4.1 family of proteins. *Biochemistry.* 41:7275–7282.

Girault, J.A., and E. Peles. 2002. Development of nodes of Ranvier. *Curr. Opin. Neurobiol.* 12:476–485.

Girault, J.A., G. Labesse, J.-P. Mornon, and I. Callebaut. 1998. The FAKs and JAKs play in the 4.1 band: a superfamily of band 4.1 domains important for cell structure and signal transduction. *Mol. Med.* 4:751–769.

Gollan, L., H. Sabanay, S. Poliak, E.O. Berglund, B. Ranscht, and E. Peles. 2002. Retention of a cell adhesion complex at the paranodal junction requires the cytoplasmic region of Caspr. *J. Cell Biol.* 157:1247–1256.

Kaplan, M.R., A. Meyer-Franke, S. Lambert, V. Bennett, I.D. Duncan, S.R. Levinson, and B.A. Barres. 1997. Induction of sodium channel clustering by oligodendrocytes. *Nature.* 386:724–728.

Kaplan, M.R., M.H. Cho, E.M. Ullian, L.L. Isom, S.R. Levinson, and B.A. Barres. 2001. Differential control of clustering of the sodium channels Na(v)1.2 and Na(v)1.6 at developing CNS nodes of Ranvier. *Neuron.* 30:105–119.

Karagogeos, D., S.B. Morton, F. Casano, J. Dodd, and T.M. Jessell. 1991. Developmental expression of the axonal glycoprotein TAG-1: differential regulation by central and peripheral neurons *in vitro*. *Development.* 112:51–67.

Kasahara, K., K. Watanabe, K. Takeuchi, H. Kaneko, A. Oohira, T. Yamamoto, and Y. Sanai. 2000. Involvement of gangliosides in glycosylphosphatidylinositol-anchored neuronal cell adhesion molecule TAG-1 signaling in lipid rafts. *J. Biol. Chem.* 275:34701–34709.

Li, X., B.D. Lynn, C. Olson, C. Meier, K.G. Davidson, T. Yasumura, J.E. Rash, and J.I. Nagy. 2002. Connexin^{29} expression, immunocytochemistry and freeze-fracture replica immunogold labelling (FRIL) in sciatic nerve. *Eur. J. Neurosci.* 16:795–806.

Malhotra, J., P. Tsiotra, D. Karagogeos, and M. Hortsch. 1998. Cis-activation of L1-mediated ankyrin recruitment by TAG-1 homophilic cell adhesion. *J. Biol. Chem.* 273:33354–33359.

Manganas, L.N., and J.S. Trimmer. 2000. Subunit composition determines Kv1 potassium channel surface expression. *J. Biol. Chem.* 275:29685–29693.

Mathis, C., N. Denisenko-Nehrbass, J.A. Girault, and E. Borrelli. 2001. Essential role of oligodendrocytes in the formation and maintenance of central nervous system nodal regions. *Development.* 128:4881–4890.

Menegoz, M., P. Gaspar, M. Le Bert, T. Galvez, F. Burgaya, C. Palfrey, P. Ezan, F. Amos, and J.A. Girault. 1997. Paranodin, a glycoprotein of neuronal paranodal membranes. *Neuron.* 19:319–331.

Milev, P., P. Maurel, M. Häring, R.K. Margolis, and R.U. Margolis. 1996. TAG-1/axonin-1 is a high-affinity ligand of neurocan, phosphacan/protein-tyrosine phosphatase-zeta/b, and N-CAM. *J. Biol. Chem.* 271:15716–15723.

Ohara, R., H. Yamakawa, M. Nakayama, and O. Ohara. 2000. Type II brain 4.1 (4.1B/KIAA0987), a member of the protein 4.1 family, is localized to neuronal paranodes. *Brain Res. Mol. Brain Res.* 85:41–52.

Pavlou, O., C. Theodorakis, J. Falk, M. Kutsche, M. Schachner, C. Faivre-Sarrailh, and D. Karagogeos. 2002. Analysis of interactions of the adhesion molecule TAG-1 and its domains with other immunoglobulin superfamily members. *Mol. Cell. Neurosci.* 20:367–381.

Pedraza, L., J.K. Haung, and D.R. Colman. 2001. Organizing principles of the axo-glial apparatus. *Neuron.* 30:335–344.

Peles, E., and J.L. Salzer. 2000. Molecular domains of myelinated axons. *Curr. Opin. Neurobiol.* 10:558–565.

Poliak, S., L. Gollan, R. Martinez, A. Custer, S. Einheber, J.L. Salzer, J.S. Trimmer, P. Shrager, and E. Peles. 1999. Caspr2, a new member of the neurexin superfamily, is localized at the juxtaparanodes of myelinated axons and associates with K^+ channels. *Neuron.* 24:1037–1047.

Poliak, S., L. Gollan, D. Salomon, E.O. Berglund, R. Ohara, B. Ranscht, and E. Peles. 2001. Localization of Caspr2 in myelinated nerves depends on axon-glia interactions and the generation of barriers along the axon. *J. Neurosci.* 21:7568–7575.

Poltorak, M., R. Sadoul, G. Keilhauer, C. Landa, T. Fahrig, and M. Schachner. 1987. Myelin-associated glycoprotein, a member of the L2/HNK-1 family of neural cell adhesion molecules, is involved in neuron–oligodendrocyte and oligodendrocyte–oligodendrocyte interaction. *J. Cell Biol.* 105:1893–1899.

Prinetti, A., S. Prioni, V. Chigorno, D. Karagogeos, G. Tettamanti, and S. Sonnino. 2001. Immunoseparation of sphingolipid-enriched membrane domains enriched in Src family protein tyrosine kinases and in the neuronal adhesion molecule TAG-1 by anti-GD3 ganglioside monoclonal antibody. *J. Neurochem.* 78:1162–1167.

Rasband, M.N., E.W. Park, D. Zhen, M.I. Arbuckle, S. Poliak, E. Peles, S.G. Grant, and J.S. Trimmer. 2002. Clustering of neuronal potassium channels is independent of their interaction with PSD-95. *J. Cell Biol.* 159:663–672.

Rios, J.C., C.V. Melendez-Vasquez, S. Einheber, M. Lustig, M. Grumet, J. Hemperly, E. Peles, and J.L. Salzer. 2000. Contactin-associated protein (Caspr) and contactin form a complex that is targeted to the paranodal junctions during myelination. *J. Neurosci.* 20:8354–8364.

Scherer, S.S., and E.J. Arroyo. 2002. Recent progress on the molecular organization of myelinated axons. *J. Peripher. Nerv. Syst.* 7:1–12.

Stolinski, C., A.S. Breathnach, B. Martin, P.K. Thomas, R.H. King, and G. Gabriel. 1981. Associated particle aggregates in juxtaparanodal axolemma and adaxonal Schwann cell membrane of rat peripheral nerve. *J. Neurocytol.* 10: 679–691.

Tait, S., F. Gunn-Moore, J.M. Collinson, J. Huang, C. Lubetzki, L. Pedraza, D.L. Sherman, D.R. Colman, and P.J. Brophy. 2000. An oligodendrocyte cell adhesion molecule at the site of assembly of the paranodal axo–glial junction. *J. Cell Biol.* 150:657–666.

Tao-Cheng, J.H., and J. Rosenbluth. 1984. Extranodal particle accumulations in the axolemma of myelinated frog optic axons. *Brain Res.* 308:289–300.

Traka, M., J.L. Dupree, B. Popko, and D. Karagogeos. 2002. The neuronal adhesion protein TAG-1 is expressed by Schwann cells and oligodendrocytes and is localized to the juxtaparanodal region in myelinated fibers. *J. Neurosci.* 22: 3016–3024.

Tsiotra, P.C., K. Theodorakis, J. Papamatheakis, and D. Karagogeos. 1996. The fibronectin domains of the neural adhesion molecule TAX-1 are necessary and sufficient for homophilic binding. *J. Biol. Chem.* 15:29216–29222.

Vabnick, I., A. Messing, S.Y. Chiu, S.R. Levinson, M. Schachner, J. Roder, C. Li, S. Novakovic, and P. Shrager. 1997. Sodium channel distribution in axons of hypomyelinated and MAG null mutant mice. *J. Neurosci. Res.* 50:321–336.

Vabnick, I., J.S. Trimmer, T.L. Schwarz, S.R. Levinson, D. Risal, and P. Shrager. 1999. Dynamic potassium channel distributions during axonal development prevent aberrant firing patterns. *J. Neurosci.* 19:747–758.

Wang, H., D.D. Kunkel, T.M. Martin, P.A. Schwartzkroin, and B.L. Tempel. 1993. Heteromultimeric K^+ channels in terminal and juxtaparanodal regions of neurons. *Nature.* 365:75–79.

Wiley, C.A., and M.H. Ellisman. 1980. Rows of dimeric-particles within the axolemma and juxtaposed particles within glia, incorporated into a new model for the paranodal glial–axonal junction at the node of Ranvier. *J. Cell Biol.* 84:261–280.

Zhou, L., C.L. Zhang, A. Messing, and S.Y. Chiu. 1998. Temperature-sensitive neuromuscular transmission in Kv1.1 null mice: role of potassium channels under the myelin sheath in young nerves. *J. Neurosci.* 18:7200–7215.

IL-1 Plays an Important Role in Lipid Metabolism by Regulating Insulin Levels under Physiological Conditions

Taizo Matsuki, Reiko Horai, Katsuko Sudo, and Yoichiro Iwakura

Center for Experimental Medicine, Institute of Medical Science, University of Tokyo, Minato-ku, Tokyo 108-8639, Japan

Abstract

IL-1 is a proinflammatory cytokine that plays important roles in inflammation. However, the role of this cytokine under physiological conditions is not known completely. In this paper, we analyzed the role of IL-1 in maintaining body weight because IL-1 receptor antagonist–deficient ($IL\text{-}1Ra^{-/-}$) mice, in which excess IL-1 signaling may be induced, show a lean phenotype. Body fat accumulation was impaired in $IL\text{-}1Ra^{-/-}$ mice, but feeding behavior, expression of hypothalamic factors involved in feeding control, energy expenditure, and heat production were normal. When $IL\text{-}1Ra^{-/-}$ mice were treated with monosodium glutamate (MSG), which causes obesity in wild-type mice by ablating cells in the hypothalamic arcuate nucleus, they were resistant to obesity, indicating that excess IL-1 signaling antagonizes the effect of MSG-sensitive neuron deficiency. $IL\text{-}1Ra^{-/-}$ mice showed decreased weight gain when they were fed the same amount of food as wild-type mice, and lipid accumulation remained impaired even when they were fed a high-fat diet. Interestingly, serum insulin levels and lipase activity were low in $IL\text{-}1Ra^{-/-}$ mice, and the insulin levels were low in contrast to wild-type mice after MSG treatment. These observations suggest that IL-1 plays an important role in lipid metabolism by regulating insulin levels and lipase activity under physiological conditions.

Key words: IL-1–deficient mouse • IL-1 receptor antagonist–deficient mouse • obese • skinny model • energy homeostasis

Introduction

IL-1 is a major mediator of inflammation. It also performs numerous functions related to host defense mechanisms, by regulating not only the immune system but also the neuronal and endocrine systems that interface with the immune system (1–3). IL-1 consists of two molecular species, IL-1α and IL-1β, both of which exert similar, but not completely overlapping, biological functions through the IL-1–type I receptor (RI). Another IL-1 receptor, the IL-1–type II receptor (RII), has also been identified, but this receptor is not considered to be involved in signal transduction; rather, it is thought to play more of a regulatory role, as a "decoy." Another member of the IL-1 gene family, IL-1 receptor antagonist (IL-1Ra), binds to IL-1 receptors without exerting agonistic activity. This molecule together with IL-1RII and the secretory forms of IL-1RI and IL-1RII are considered to be negative regulators of IL-1 signaling, participating in the complex regulation of IL-1 activity. IL-1 is produced by a large variety of cells, including monocytes/macrophages, epithelial and endothelial cells, and glial cells. IL-1Rs are also expressed on a wide range of cells of the immune, neural, and endocrine systems, reflecting the pleiotropic activities of this molecule (4).

We have shown that both IL-1α and IL-1β are induced in the brain of a mouse after injection with turpentine. The stress response against turpentine injection as determined by the development of fever and secretion of glucocorticoid is abolished in IL-1α/β double-deficient ($IL\text{-}1^{-/-}$) mice, suggesting that endogenous brain IL-1 plays important roles in the stress response (5). Endogenous brain IL-1 also plays a pivotal role in the development of anorexia and hypothalamic cytokine expression upon administration with LPS (6). Interestingly, IL-1 is constitutively expressed

Address correspondence to Yoichiro Iwakura, Center for Experimental Medicine, Institute of Medical Science, University of Tokyo, Shirokanedai, Minato-ku, Tokyo 108-8639, Japan. Phone: 81-3-5449-5536; Fax: 81-3-5449-5430; email: iwakura@ims.u-tokyo.ac.jp

Abbreviations used in this paper: ARH, arcuate nucleus in the hypothalamus; BAT, brown adipose tissue; CRF, corticotropin releasing factor; FFA, free fatty acid; IL-1Ra, IL-1 receptor antagonist; $IL\text{-}1^{-/-}$, IL-1α/β double-deficient; $IL\text{-}1Ra^{-/-}$, IL-1Ra–deficient; LPL, lipoprotein lipase; MC3/4R, melanocortin-3/4 receptor; MSG, monosodium glutamate; PHP, post-heparin plasma; POMC, pro-opiomelanocortin; RI, type I receptor; RII, type II receptor; TAG, triacylglycerol; TC, total cholesterol; UCP, uncoupling protein; VCO_2, carbon dioxide production; VO_2, oxygen consumption; WAT, white adipose tissue.

 J. Exp. Med. © The Rockefeller University Press • 0022-1007/2003/09/877/12 $8.00
Volume 198, Number 6, September 15, 2003 877–888
http://www.jem.org/cgi/doi/10.1084/jem.20030299

in health in specific areas of the brain, including the hypothalamus of humans and rodents (7, 8), and IL-1RI is also expressed in the brain, notably in the endothelial cells of blood vessels in the hippocampus and hypothalamus (9, 10). Because locomotive activity of IL-1α/β$^{-/-}$ mice was lower than control mice (11) and sleep regulation was abnormal in IL-1$^{-/-}$ mice as well as in IL-1RI$^{-/-}$ mice (12, 13), brain IL-1 may play important regulatory roles in maintaining homeostasis of the host under physiological conditions.

We found recently that IL-1Ra gene–deficient (IL-1Ra$^{-/-}$) mice are lean and show growth retardation, suggesting that IL-1 may also be involved in energy homeostasis (5). In this context, IL-1 was reported to be involved in the feeding suppression caused by leptin, which is released from adipocytes and suppresses food intake through actions in the hypothalamus (14–17). IL-1 promotes the release of corticotropin releasing factor (CRF; references 18, 19), melanocortins, and other neuropeptides (4). CRF suppresses feeding behavior when administered intracerebroventricularly (20, 21). However, mice lacking both CRF RI and RII do not show any abnormal feeding behavior, indicating that the absence of CRF signaling does not accelerate feeding (22). On the other hand, excess IL-1 signaling induced by exogenously administered IL-1 or by leptin suppresses feeding behavior through a mechanism involving central melanocortin-3/4 receptors (MC3/4Rs; reference 23). Furthermore, mice with knockouts of MC3/4Rs develop mature-onset obesity (24–26), and likewise, mice lacking the pro-opiomelanocortin (POMC) gene, which encodes the precursor of an endogenous agonist for MC3/4Rs (α-melanocyte stimulating hormone), also develop obesity (27). Thus, these receptor signals are crucial for the feeding regulation under physiological conditions. However, it is not known whether IL-1, which is detected in the brain under physiological conditions, plays any role in the regulation of feeding behavior through these receptors.

IL-1 has also been suggested to be involved in peripheral energy homeostasis through endocrine mechanisms. IL-1β selectively destroys the insulin-producing β cells, but not the α cells, in vitro (28). This cytotoxic effect of IL-1 is suggested to be mediated by the induction of inducible nitric oxide synthase or prostaglandins (29–31). On the other hand, it was reported that IL-1 acts as a hypoglycemic agent not only in normal animals but also in alloxan-induced diabetic and genetically diabetic mice (32) and increases insulin and glucagon levels, suggesting that IL-1 has antidiabetic effects (33). Thus, the effects of IL-1 on glucose and insulin metabolism are somewhat conflicting, probably reflecting differences in experimental conditions.

Moreover, IL-1 has been suggested to directly modulate lipid metabolism by suppressing the activity of lipoprotein lipase (LPL), the enzyme regulating the disposal of lipid fuels in the body (34, 35). IL-1 may also regulate adipocyte function, as IL-1 inhibits adipocyte maturation and the synthesis of fatty acid transport proteins in adipose tissue in vitro (36, 37). These findings indicate that the IL-1/IL-1Ra system may control lipid and lipoprotein metabolism through direct actions on adipose tissues. However, it remains unclear whether IL-1 is involved in energy homeostasis under physiological conditions and, if so, the mechanism involved is unknown.

To elucidate the role of the IL-1 system in energy homeostasis in this paper, we examined feeding behavior and peripheral metabolic changes of IL-1$^{-/-}$ and IL-1Ra$^{-/-}$ mice under physiological conditions and in response to manipulating food intake. The results suggest that IL-1 plays an important role in energy homeostasis under physiological conditions, acting via a peripheral mechanism.

Materials and Methods

Animals and Diets. IL-1Ra$^{-/-}$ and IL-1$^{-/-}$ mice were produced by homologous recombination as described previously (5). These mice were backcrossed to the C57BL/6J strain mice for eight generations. Mice were housed individually from weaning at 3 wk old, and were allowed free access to chow and water, except when described separately. Mice were kept under specific pathogen-free conditions in an environmentally controlled clean room at the Center for Experimental Medicine, Institute of Medical Science, University of Tokyo. They were housed at an ambient temperature of 24°C and a daily cycle of 12 h light and darkness (8:00–20:00). All experiments were performed according to the institutional ethical guidelines for animal experiments and according to the safety guidelines for gene manipulation experiments.

Body weight and food intake were measured in the morning, at least twice a week, beginning from the day of weaning. 20-wk-old mice were killed, and white adipose tissue (WAT) and interscapular brown adipose tissue (BAT) pads were dissected and weighed. Intraperitoneal body temperature was measured as described previously (5). Food restriction of male mice at 8 wk old was performed for 18 d by feeding mice 0.9 g of normal chow each day. In food shift experiments, mice were fed a normal chow diet (fat, 5.1%; total energy, 4.18 kcal/g) or a high-fat normocaloric diet (fat, 23.6%; total energy, 4.55 kcal/g) from 9 to 17 wk old.

For hypothalamic lesion–induced obesity, newborn mice were administered either saline or monosodium glutamate (MSG) (4 mg/g body weight/day) i.p., from postnatal days 1 to 7 (38, 39). Body weight and food intake were measured in the morning once a week up to 20 wk old, the mice were killed, and serum and WAT were collected for measuring insulin level and WAT weight.

Indirect Calorimetry. Amount of oxygen consumption (VO_2) and carbon dioxide production (VCO_2) were simultaneously determined by indirect calorimetry using Respina (IH26; NEC Sanei Instruments Ltd.). Male mice at 15 wk old were housed in separate chambers for 1 h before the experiment. 10-min measurements were performed three times every 60 min during the middle of the light cycle (11:00–17:00) under a constant air-flow rate (200 ml/min). VO_2 and VCO_2 were calculated from the oxygen consumption and carbon dioxide production curves using the constant regions corresponding to resting period.

Fasting Experiments. To examine expression levels of neuropeptides and uncoupling proteins (UCPs), age-matched mice (6–8 wk old) were divided into three groups (n = 4 per group). The fed group was allowed to feed ad libitum, the fasted group was fasted for 48 h, and the refed group was allowed to feed freely for 4 h after a 48-h fast. Mice were allowed free access to water during these experiments. Mice were killed, and brain and

peripheral tissues were dissected. Northern blot analyses for total RNA and poly (A)$^+$ RNA were performed as described previously (5). β-Actin was used as an internal control.

Probes. Probes for Northern blot hybridization were amplified by PCR with the following specific primers, using mouse hypothalamus and WAT cDNA as templates: agouti gene–related protein sense: 5′-ATGCTGACTGCAATGTTGCTG-3′, antisense: 5′-CTAGGTGCGACTACAGAGGTT-3′; cocaine–amphetamine-regulated transcript sense: 5′-ATCGAAGCGTTGCAAGAAGT-3′, antisense: 5′-GGAATATGGGAACCGAAGGT-3′; melanin-concentrating hormone sense: 5′-ATGGCAAAGATGACTCT-CTCT-3′, antisense: 5′-GACTTGCCAACATGGTCGGTA-3′; POMC sense: 5′-GCTTGCATCCGGGCTTGCAA-3′, antisense: 5′-TCACTGGCCCTTCTTGTGCG-3′; UCP1 sense: 5′-ATGGTGAACCCGACAACTTC-3′, antisense: 5′-TTATGTG-GTACAATCCACTG-3′; UCP2 sense: 5′-ATGGTTGGTTT-CAAGGCCAC-3′, antisense: 5′-TCAGAAAGGTGCCTCCC-GAG-3′; UCP3 sense: 5′-ATGGTTGGACTTCAGCCCTC-3′, antisense: 5′-TCAAAACGGAGATTCCCGCA-3′; resistin sense: 5′-AGCTGTGGGACAGGAGCTAA-3′, antisense: 5′-CCTG-

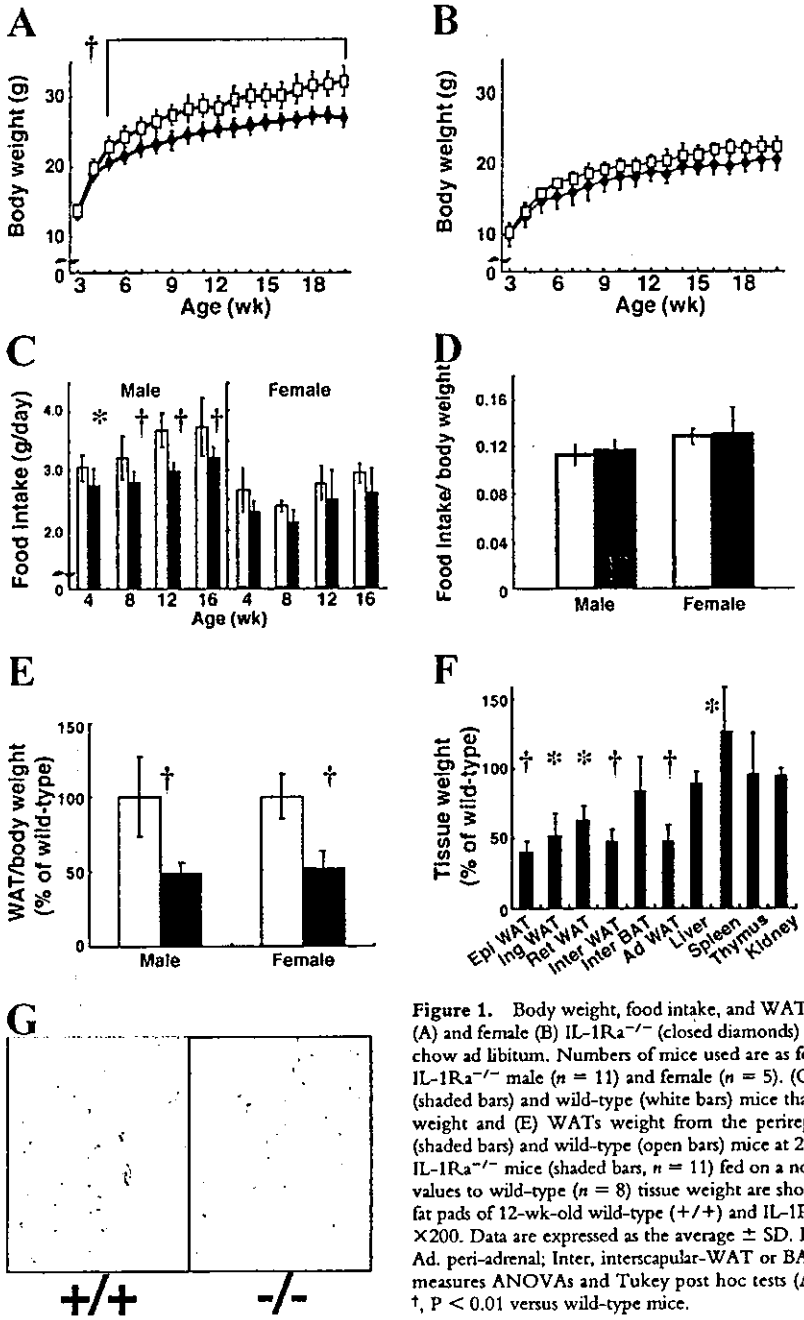

Figure 1. Body weight, food intake, and WAT weight in IL-1Ra$^{-/-}$ mice. Growth curves of male (A) and female (B) IL-1Ra$^{-/-}$ (closed diamonds) and wild-type mice (open squares), fed on a normal chow ad libitum. Numbers of mice used are as follows: wild-type male (n = 8) and female (n = 5); IL-1Ra$^{-/-}$ male (n = 11) and female (n = 5). (C) Daily food intake of male and female IL-1Ra$^{-/-}$ (shaded bars) and wild-type (white bars) mice that are shown in A and B. (D) Food intake per body weight and (E) WATs weight from the perireproductive tissues per body weight of IL-1Ra$^{-/-}$ (shaded bars) and wild-type (open bars) mice at 20 wk old. (F) Fat pads and various tissues from male IL-1Ra$^{-/-}$ mice (shaded bars, n = 11) fed on a normal chow were weighed at 20 wk old, and relative values to wild-type (n = 8) tissue weight are shown. (G) Paraffin sections of WAT from epididymal fat pads of 12-wk-old wild-type (+/+) and IL-1Ra$^{-/-}$ (−/−) mice. Hematoxylin and eosin staining. ×200. Data are expressed as the average ± SD. Epi, epididymal; Ing, inguinal; Ret, retroperitoneal; Ad. peri-adrenal; Inter, interscapular-WAT or BAT. Statistical significance was calculated by repeated measures ANOVAs and Tukey post hoc tests (A–C), and by Student's t tests (D–F). *, $P < 0.05$, †, $P < 0.01$ versus wild-type mice.

TAGAGACCGGAGGACA-3′; adiponectin sense: 5′-GCACG-AGGGATGCTACTGTT-3′, antisense: 5′-CCATACACCTG-GAGCCAGAC-3′. The probe for mouse leptin was a generous gift from K. Nakao (Kyoto University, Kyoto, Japan), and those for rat neuropeptide Y and rat pro-orexin were from T. Sakurai (Tsukuba University, Tsukuba, Japan).

Blood Constituents. To analyze blood constituents, 9–10-wk-old mice were used. Blood samples were collected by retro-orbital puncture under anesthesia at indicated times. Blood glucose levels and serum triacylglycerol (TAG), free fatty acid (FFA), and total cholesterol (TC) levels were measured by the glucose oxidase method (Terumo Co.) and by colorimetric assays (triglyceride-L test, NEFA-C test [Wako Pure Chemical Industries Ltd.]; Determiner TC 555 [Kyowa Medex Co.]), respectively. Serum insulin and leptin levels were both measured by ELISA (Seikagaku Co.).

Post-Heparin Plasma (PHP) Lipase Activity. Male mice at 9–11 wk old were fasted from one day before the experiment, i.v. injected with 100 U/kg body weight of heparin, and plasma were collected 5 min later. Total and hepatic lipase activities

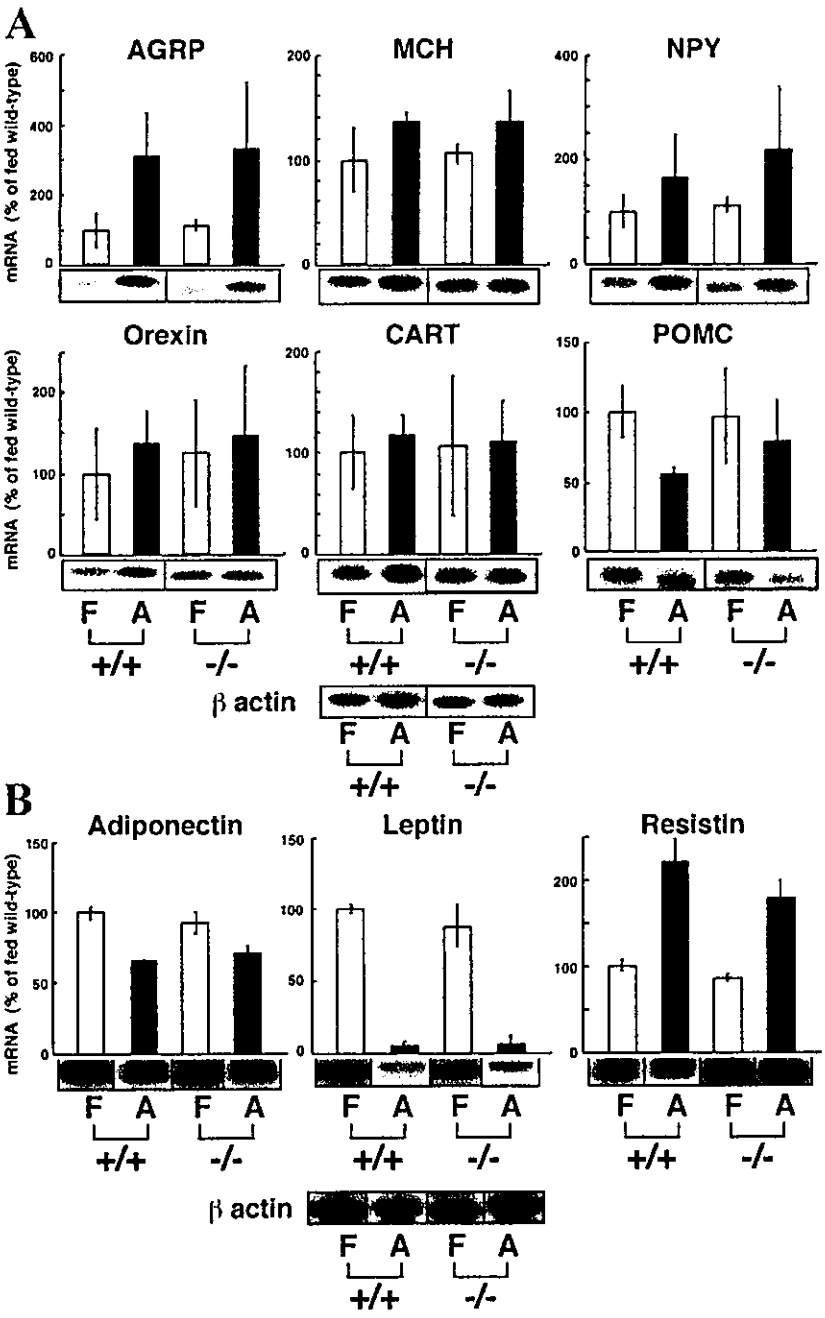

Figure 2. Normal expression of hypothalamic peptides and adipo-cytokines after fasting in IL-1Ra$^{-/-}$ mice. (A) 5 μg poly (A)$^+$RNAs from the hypothalamus of fed or fasted mice (four mice for each lane) were purified, and Northern blot hybridization was performed with indicated probes. (B) 20 μg total RNAs from epididymal WAT were prepared, and hybridized with indicated probes. F, fed ad libitum (white bars), A, fasted for 48 h (shaded bars). +/+, wild-type mice, −/−, IL-1Ra$^{-/-}$ mice. Autoradiographs are representative in three independent experiments using at least four animals in one group. Data are expressed as the average ± SD of all the experiments.

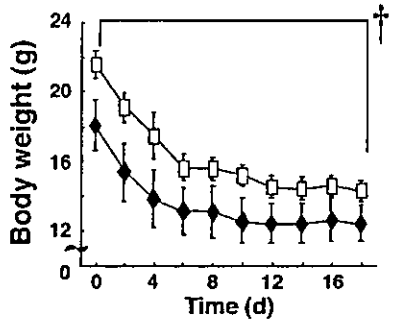

Figure 3. Impairment of energy storage in IL-1Ra$^{-/-}$ mice. Body weight changes of age-matched wild-type (open squares, $n = 5$) and IL-1Ra$^{-/-}$ (closed diamonds, $n = 5$) male mice under food restriction (0.9 g/day of a normal chow). Data are expressed as the average ± SD. †, $P < 0.01$ versus wild-type mice

were measured using lipase activity assay kit (Progen Biotech).

Glucose Tolerance Test and Insulin Tolerance Test. For the glucose tolerance test, 8–12-wk-old mice were fasted from the previous day and injected i.p. with 1.5 mg/g body weight glucose. For the insulin tolerance test, mice were fasted for a day and injected i.p. with 0.75 mU/g body weight human recombinant insulin (Sigma-Aldrich). Blood samples were collected by retro-orbital puncture.

Histological Examination. Adipose tissue and pancreas of 9–10-wk-old mice were fixed by 10% phosphate-buffered formalin and embedded in paraffin. 10-μm sections were stained with hematoxylin/eosin.

Statistical Analysis. All values were calculated as average ± SD. Comparisons were made using the Student's *t* test, one-way, or repeated measures ANOVA, Fisher's PLSD, or the Tukey post hoc test, when appropriate.

Results

Growth, Food Intake, and Body Weight of IL-1Ra$^{-/-}$ Mice. To elucidate the role of IL-1 in body weight and energy homeostasis, we examined the growth of IL-1Ra$^{-/-}$, IL-1$^{-/-}$, and wild-type littermate mice. IL-1$^{-/-}$ mice showed normal weight gain until 20 wk old, in both males and females (reference 5 and unpublished data). Growth of IL-1Ra$^{+/-}$ (heterozygous) mice was also similar to wild-type mice (unpublished data). On the other hand, the body weight and daily food intake of IL-1Ra$^{-/-}$ male mice were lower than those of wild-type mice at 4 wk old, and the difference in body weight increased with age (Fig. 1, A and C). The body weight and daily food intake of IL-1Ra$^{-/-}$ female mice were also lower than those of wild-type mice, although the difference was not statistically significant (Fig. 1, B and C). However, food intake per gram body weight was similar between IL-1Ra$^{-/-}$ and wild-type mice, suggesting that the reduced food intake in mutant animals may reflect the difference in body weight (Fig. 1 D). These observations indicate that a lack of IL-1 signaling is dispensable in the maintenance of body weight, but that excess IL-1 signaling, due to IL-1Ra deficiency, suppresses weight gain under physiological conditions.

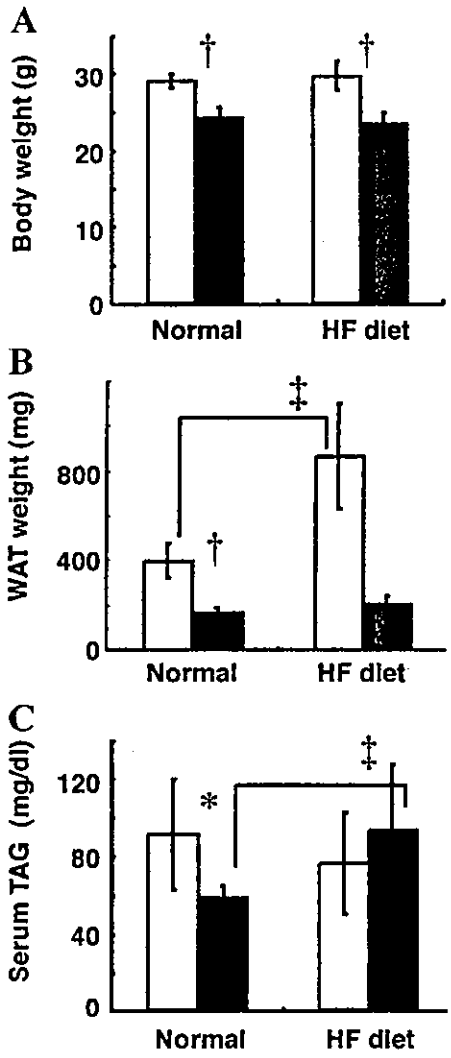

Figure 4. Impairment of lipid accumulation into WATs in IL-1Ra$^{-/-}$ mice. Mice were fed with a normal chow (Normal) or a high-fat diet (HF diet) for 8 wk. Body weight (A), epididymal WAT mass (B), and serum TAG level (C) were compared between normal chow and high-fat diet groups. IL-1Ra$^{-/-}$ (shaded bars, $n = 5$) and wild-type (white bars, $n = 5$) mice at the age of 17 wk were used. Data are expressed as the average ± SD. Statistical significance was determined by one-way ANOVAs and Fischer's PLSDs. *, $P < 0.05$, †, $P < 0.01$ versus wild-type mice fed with the same chow. ‡, $P < 0.01$ versus the same genotype mice fed with a normal chow.

The fat mass per body weight of male IL-1Ra$^{-/-}$ mice was less than half that of wild-type mice (Fig. 1 E). Histological analysis of adipose tissue, however, revealed that adipocytes of IL-1Ra$^{-/-}$ mice under fed conditions exhibited normal morphology and cell volume compared with those of wild-type mice (Fig. 1 G), suggesting that adipocyte differentiation was not altered in IL-1Ra$^{-/-}$ mice. Female IL-1Ra$^{-/-}$ mice also had significantly less fat mass than wild-type mice (Fig. 1 E), although their body weights were similar (Fig. 1 B). These results suggest that fat storage is

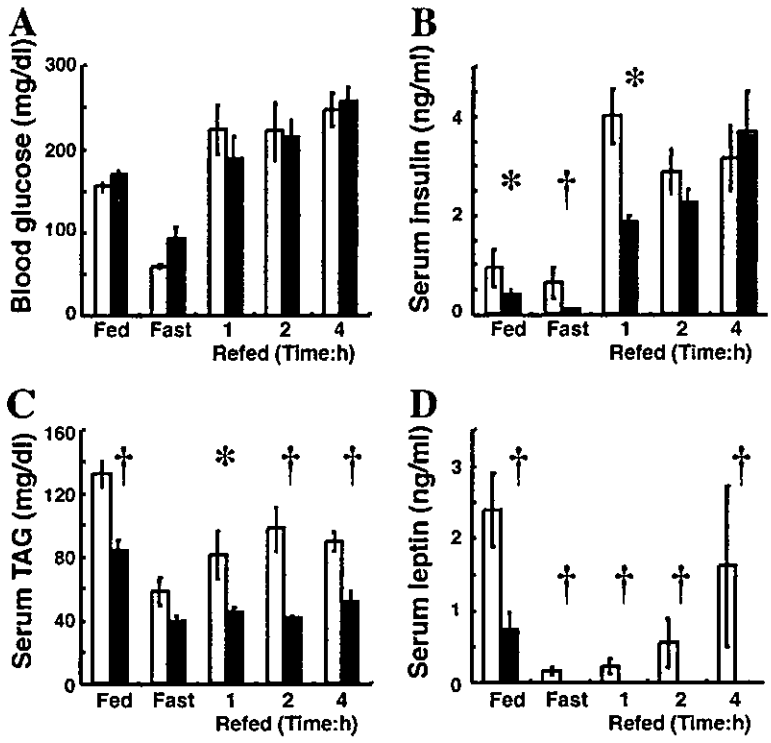

Figure 5. Decreased serum levels of insulin, TAG, and leptin in IL-1Ra$^{-/-}$ mice. Blood glucose (A), serum insulin (B), TAG (C), and leptin (D) levels in body weight matched wild-type (8 wk old, white bars) and IL-1Ra$^{-/-}$ (15 wk old, shaded bars) mice were measured. "Fed" samples were collected from mice fed ad libitum 2 d before fasting. "Fasted" samples were collected after 48 h of fasting, and refeeding started (0 h). Data are expressed as the average ± SD, and are reproducible for three independent experiments using at least four mice in each genotype. Statistical significance was determined by Student's *t* tests. *, $P < 0.05$, †, $P < 0.01$ versus wild-type mice.

impaired in IL-1Ra$^{-/-}$ mice. No difference was observed in the weights of other tissues between IL-1Ra$^{-/-}$ and wild-type mice, except for the spleen, which was increased in size in IL-1Ra$^{-/-}$ mice (Fig. 1 F).

Expression of Energy Regulatory Factors in Peripheral Tissues. We assessed the regulation of energy expenditure in the periphery. Expression levels of UCPs (UCP1, UCP2, and UCP3), which are involved in heat production via the uncoupling of oxidative metabolism from ATP generation in BAT, WAT, and skeletal muscles, were compared. We found that UCP expression levels were normal in IL-1Ra$^{-/-}$ mice (unpublished data). Moreover, basal body temperature of IL-1Ra$^{-/-}$ mice was similar to wild-type mice (wild-type mice: 37.8 ± 0.6°C, $n = 9$; IL-1Ra$^{-/-}$ mice: 37.5 ± 0.7°C, $n = 9$, $P = 0.29$). Changes in body temperature in response to fasting or cold stress (at 4°C for 6 h) were also similar to those of wild-type mice (unpublished data). Although locomotive activity in IL-1Ra$^{-/-}$ mice, as assessed by the open-field test, was slightly lower than that of wild-type mice, motor function, as evaluated by the rota-rod test, was similar between IL-1Ra$^{-/-}$ and wild-type mice (unpublished data).

Furthermore, we examined energy expenditure using indirect calorimetry. VO_2 and VCO_2 of IL-1Ra$^{-/-}$ mice were somewhat lower compared with wild-type mice, although the difference was not statistically significant (VO_2 wild-type mice: 60.5 ± 8.2 ml/kg/min, $n = 13$; IL-1Ra$^{-/-}$ mice: 52.2 ± 11.8 ml/kg/min, $n = 8$, $P = 0.053$; VCO_2 wild-type mice: 53.2 ± 12.3 ml/kg/min, $n = 13$; IL-1Ra$^{-/-}$ mice: 44.9 ± 15.9 ml/kg/min, $n = 8$, $P = 0.094$ average ± SD). However, respiratory exchange ratio was normal (wild-type mice: 0.845 ± 0.094, $n = 13$; IL-1Ra$^{-/-}$ mice: 0.853 ± 0.148, $n = 8$, $P = 0.56$). These data suggested that the energy expenditure in IL-1Ra$^{-/-}$ mice is not elevated and energy expenditure mechanisms are normal in IL-1Ra$^{-/-}$ mice under physiological conditions.

We also examined the expression levels of the adipocyte-derived cytokines (adipo-cytokines), adiponectin, leptin, and resistin, which are involved in lipid and glucose metabolism and insulin resistance (Fig. 2 B). No differences in expression levels of these adipo-cytokines were detected between IL-1Ra$^{-/-}$ and wild-type mice, suggesting that these adipo-cytokines are not involved in the decreased energy storage in IL-1Ra$^{-/-}$ mice.

Expression of Energy Regulatory Factors in the Central Nervous System. To elucidate whether or not hypothalamic feeding suppression mechanisms are involved in the lean phenotype of IL-1Ra$^{-/-}$ mice, we analyzed the expression levels of energy regulatory factors in the brain. We examined the expression levels of agouti gene–related protein (AGRP), melanin-concentrating hormone (MCH), neuropeptide Y (NPY), and orexin mRNAs as orexigenic peptides, and cocaine–amphetamine-regulated transcript (CART) and POMC mRNAs as anorexigenic factors using hypothalami from either ad libitum–fed mice or from 48-h fasted mice (Fig. 2 A). No significant differences between wild-type and IL-1Ra$^{-/-}$ mRNA levels were observed, however, under either fed or fasted conditions. These results show that the expression of major hypothalamic factors regulating feeding behavior is normal in IL-1Ra$^{-/-}$ mice.